CEAC-TR-01-0108

LEAKAGE FAILURE MODES AND MECHANICS OF THREADED FIBER-COMPOSITE JOINTS UNDER COMBINED INTERNAL PRESSURE, AXIAL AND MAKEUP LOADING

S. S. Wang and X. H. Chen

Composites Engineering and Applications Center (CEAC),
University of Houston, Houston, TX.

JANUARY 2001

COMPOSITES ENGINEERING AND APPLICATIONS CENTER
FOR PETROLEUM EXPLORATION AND PRODUCTION

UNIVERSITY OF HOUSTON
HOUSTON, TX 77204-0900

CEAC-TR-01-0108

LEAKAGE FAILURE MODES AND MECHANICS OF THREADED FIBER-COMPOSITE JOINTS UNDER COMBINED INTERNAL PRESSURE, AXIAL AND MAKEUP LOADING

By

S. S. Wang* and X. H. Chen**

Composites Engineering and Applications Center (CEAC), and
Department of Mechanical Engineering
University of Houston
4800 Calhoun Road
Houston, TX 77204-0903

January, 2001

* Distinguish Professor and Director
** Research Associate

Table of Contents

Abstract

In this report, a comprehensive analytical study has been conducted to investigate the leakage resistance of threaded fiber composite tubular joints under combined internal pressure, axial loading, and mechanical make-up turns. A detailed analytical model, based on a 3-D stress formulation, has been established to model local thread stress concentrations, thread surface contact, and composite material damage in the composite joints with asymmetric thread configurations. Nonlinear composite material constitutive equations, slip-stick interface contact mechanics, and physical-mechanism-based failure theory and composite degradation are all included in the formulation of the problem. An incremental-iterative computational mechanics algorithm has further been developed to simulate the leakage failure processes in the threaded joints with different combinations of applied pressure, axial loading and make-up loading. Leakage resistance of a threaded composite joint is studied with the aid of both the joint functional failure criteria, i.e., loss of thread-surface bearing pressure, and the recently developed composite material failure theory, i.e., progressive material damage in composite laminate plies through the joint wall thickness direction.

The analytical model and the method of analysis have been utilized to evaluate the leakage failure resistance of threaded SPH tubular fiberglass composite joints with nonsymmetrical threads subject to combined axial loading, internal pressure and make-up turns. Analytical predictions of the threaded composite tubular joint have been compared with experimental test results conducted elsewhere. Excellent agreement is obtained in the comparison. For a threaded SPH joint under any combinations of external loading and make-up turns, one can construct a complete leakage failure resistance map for the joint, based on the proposed bearing-pressure failure criteria and the mechanism-based composite material damage and failure criteria. The important effects of joint make-up turns, hoop-to-axial stress biaxiality ratio (i.e., external loading mode), thread surface friction coefficient, and relative variations of pin and box section thicknesses on the composite joint leakage failure have been quantitatively determined in detail. In conjunction with the thread tightening factor and the joint safety factor introduced in the study, an important engineering formula has also been established from the numerical results for the SPH joints to relate the joint leakage resistance and its failure modes to different joint geometry and combinations of make-up turns, pipe internal pressure, and axial loading.

1. INTRODUCTION

Corrosion-resistant, fiber-reinforced polymer composite pipe has been utilized extensively in various oil and gas field exploration and production (E & P) operations with aggressive environments. Joining the composite pipes with threaded connections has been commonly employed at present. The complex geometry of threads, high concentrations from local stress transfer, and nonlinear, anisotropic fiber composite properties have caused concerns on structural integrity and functional reliability of the threaded composite joints, especially those in large-diameter pipes under high pressure and complex make-up loading.

It is recognized that safe design for threaded joints in metallic pipes has been performed for a long time. Most of the design methodologies used for metallic threaded joints have been well established and documented. However, fundamental mechanics of threaded composite joining and its integrity remains less understood. At present, rigorous analytical models and predictive methodologies to ensure leak-free design and performance, especially long term, of threaded fiber-composite pipe joints simply do not exist. In most cases, large-scale, expensive hydrostatic burst tests have to be used to evaluate the composite joint integrity under selected pressure and makeup loading. This practice is expensive, time-consuming, and yields only limited understanding and test data without providing any predictive capability of the composite joint failure resistance.

The difficulties involved in this situation arise from the following complexities of the problem:

(1). Material anisotropy and nonlinearity of fiber composites in both pipe and joints.
(2). Lack of understanding of the local contact mechanics of a threaded joint.
(3). Complex leakage failure modes due to material damage and loss of thread bearing pressure.
(4). Unknown relationships among local stress concentrations in threads, thread surface bearing-pressure sealing, material damage and degradation, and external multi-axial loading modes.
(5). Lack of accurate threaded composite joint mechanics analysis and design methods.

It is obvious that composite material properties, and thread geometry and functions used in a composite tubular joint are different from those in a metallic joint. While various thread configurations have been used in connecting tubular fiber composite pipes, they all serve two common functions, i.e., structural load transfer and contact pressure sealing, and possess unique features in the joint performance evaluation. These features may include, but not limited to, the following:

(1). Local thread tapering and mechanical makeup interference.
(2). Thread surface contact pressure and its sealing capability.
(3). Local 3-D stress concentrations in threads and along the contact surface.
(4). Interactions among local thread deformation and stress, combinations of axial, pressure and makeup loading, and leakage failure modes.

Given these complications and unique features of the problem, it becomes clear that predictive analytical models and advanced mechanics analysis/design, based on rigorous composite mechanics, failure theories, nonlinear contact mechanics and advanced computational methods, may provide the only viable approach to resolve the concerns. The present study is aimed at understanding the composite threaded joint failure behavior and developing predictive relationships to relate the joint leakage failure to various thread geometry, lamination parameters, material and loading variables of the thread composite joint.

A significant amount of effort is made to:

(1). Further develop the composite-joint failure mechanics analysis method previously established to address complex asymmetric thread configurations.

(2). Based on the model and the method developed, to determine leakage failure modes and associated failure criteria for fiber composite joints with asymmetric threads in conjunction with the hydrostatic burst tests conducted elsewhere.

(3). Provide quantitative leakage failure-resistant maps for safe design of threaded composite joints under different combinations of pressure loading and make-up turns.

(4). Establish accurate engineering relationships (or formulas) among joint deformation, thread bearing pressure, leakage failure modes, and various combinations of internal pressure, axial loading, and makeup interference.

In the next section, a review is conducted on the literature to identify the analytical and experimental work on tubular threaded joints previously conducted, including both metallic and composite joints. The objectives and the scope of the present study are given in Section 3. In Section 4, mathematical formulation is made for the boundary-value problem of a composite joint with asymmetric threads under general external loading, including internal pressure, axial loading and make-up turns. For the convenience of later discussion of the composite joint leakage resistance and safe design, a thread tightening factor and a joint leakage safety factor are introduced and defined in Section 5. Computational mechanics models and methods are developed in Section 6 for accurate evaluation of composite joint deformation with progressive damage and thread bearing failure (i.e., loss of bearing contact pressure and thread material damage). Detailed numerical results are given for several cases of composite SPH joint deformation and leakage failure modeling under various combinations of internal pressure, axial loading and make-up turns. The effects of different loading modes, makeup turns, thread surface friction, and pin and box section-thickness variations are determined quantitatively. Leakage failure (or resistance) maps with different structural and functional failure modes are constructed and compared with experimental data obtained from the composite joint tests conducted elsewhere. Based on the results obtained, important relationships among thread bearing pressure, make-up turns, and applied pressure and axial loading are established. These relationships are constructed in simple engineering formulas, which can be effectively and conveniently used for safe design for leakage failure resistance of threaded composite joints under any combinations of axial, pressure and makeup loading.

2. LITERATURE REVIEW

2.1 Stress Analysis of Bolted and Threaded Metallic Connectors

Many researchers have conducted investigations on the load bearing capacity of threaded metal fasteners since Den Hartog (1929) first examined the subject of bolts holding a stack of plate rotors in a turbo-generator. In the analysis developed by Bretl and Cook (1979), all the threads are replaced with an equivalent load-transfer layer of orthotropic properties. Dragoni (1992) recently made a comprehensive study on the effects of thread pitch and friction on stress concentrations in a metallic bolt-nut connection, using an axisymmetric finite element model.

For a threaded metallic connection, instead of treating the threaded bolt-nut joint as an axisymmetric solid, Rhee (1990) analyzes its deformations with a 3-D solid model. The results indicate that a 2-D model may underestimate the critical stresses in the metallic threaded bolt-nut joint by approximately 20%, when compared with the 3-D model for the joint containing threads with a helical angle of 5°.

Using a finite element method, Macdonald and Deans (1995) conduct a detailed stress analysis of threaded connections in drill strings and bottom-hole assemblies. Considering the threads with a generic trapezoidal shape, they have established relationships among the nominal load, resulting stress concentrations, and local elastic deformations at the roots of critical threads.

2.2 Analysis of Threaded Tubular Metal Joints

Tubular joint threads behave differently from those in a bolt-nut joint in both geometry and load transfer. Threads in a tubular joint not only transfer loads between pin and box sections in a complicated way, but also provide the needed sealing capacity to prevent the joint from leakage. Of particular interest are the makeup interference and its effect on the leakage failure in a threaded connection. Weiner and Sewell (1967) examine the sealing mechanisms of threaded metallic tubular joints and conclude that a leakage failure criterion, involving only torque in makeup, is not reliable. Day, Moyer and Hirshberg (1989) develop a method to establish a proper torque-position criterion for API eight-round casing and tubing threads. Finite element simulations are also conducted for the thread connections. Hilbert and Kalil (1992) evaluate a premium threaded metallic connection by a combined approach, using axisymmetric finite element modeling and full-scale testing.

2.3 Analysis of Composite Joints

Sun, et al (1997) study the effects of lateral constraints and clamping pressure on the response of bolted composite joints during bearing failure. With the aid of the ABAQUS software, they analyze the responses and failure of the joints with a pin-loaded hole (no constraints), fastened joints with washers, and fastened joints without washers. Most recently, Jones et al (1999) have obtained the results of a series of experimental,

analytical and numerical studies on matrix-dominated failure of bonded joints, composite repairs, and rib-stiffened postbuckled structures.

2.4 Failure Study on Threaded Composite Joints

While many studies have been conducted on fiber composite tubing bodies (Swanson, Messick & Tian, 1987; Daniel & Ishai, 1994; and Wang & Srinivasan, 1996), very limited work has focused on mechanical reliability of threaded composite tubular connections. Dilintas (1991) conduct a study on a threaded composite tubing connection under several different loading. Frictionless contact, linear elastic material properties and the simple maximum stress failure criterion are assumed in the study. Note that the maximum stress criterion does not account for interactions among multiaxial stress components during deformation and failure of the joint. Dilintas (1992) also investigate the influence of filament winding angle on the performance of a threaded composite joint.

Wang and Lu (1996) conduct a detailed study with combined experiments and analytical modeling of leakage failure in threaded fiber composite joints under combined internal pressure, axial and makeup loading. The study includes nonlinear ply composite constitutive equations, local thread contact mechanics, progressive material degradation, and physical mechanism-based ply-failure criteria. Based on the local contact and failure mechanics modeling, various leakage-failure modes in threaded composite joints are identified and predicted. More importantly, a mechanism-based leakage failure envelope is established for the threaded composite joint subject to general applied loading. Based on the joint leakage failure experiments, the leakage-resistant reliability of the threaded composite joint has been determined quantitatively by the use of the leakage failure mechanics theory and models.

3. OBJECTIVES AND SCOPE OF THE STUDY

The objectives of the research are to:

1) Predict leakage failure of the threaded composite joints considered here under combined internal pressure, axial tension and makeup loading.
2) Establish quantitative relationships between thread bearing pressure and applied loading on the joint (i.e., internal pressure, axial tension and makeup turns).
3) Determine quantitatively the effect of joint geometry (i.e., thicker box and thinner pin sections), makeup turns, friction on joint leakage failure envelopes under combined internal pressure, axial tension and make-up loading.

To achieve these objectives, the following technical tasks have been conducted, and the results are obtained and described in this report.

1) Proper formulation and analytical modeling of the threaded composite joint problem under combined external loading. The formulation includes nonlinear anisotropic ply constitutive equations, failure criteria for fiber- and matrix-dominated cracking modes in the tube body and threads, thread-tube body interface debonding, and sealing failure caused by the thread-contact bearing pressure loss.
2) Developing rigorous mechanics algorithm and solution procedure for modeling progressive damage and failure in the threaded fiber composite joint, based on physical mechanisms and micromechanics of heterogeneous media.
3) Determining quantitatively leakage failure envelopes for the threaded composite joint under combined internal pressure, axial tension and makeup loading.
4) Investigating the effects of composite threaded joint geometry, contact friction, and applied loading modes on the composite joint leakage failure.

4. FORMULATION FOR BOUNDARY-VALUE PROBLEM OF THREADED COMPOSITE JOINTS

4.1 Assumptions and Approximations

A salient feature of a threaded tubular composite joint is the axisymmetry of its global structural geometry. The effect of nonsymmetric helical threads depends on the helical angle, which is a function of the joint diameter and the thread pitch. In this study, the thread helical angle (0.54°) is small (For the SPH joint considered here, the internal diameter of the tube body is 8.42 inch with a thread pitch 0.25 inch as shown in Fig.4-1). The threaded composite tubular joint is modeled as a geometrically axisymmetric solid structure with all the threads initially in contact (Fig.4-1).

The composite joint is subject to general axisymmetric loading, including internal pressure, axial loading and make-up turns. Ply material constitutive equations for the filament-wound composite are assumed to be transversely isotropic in principal material coordinates. A commonly used glass/epoxy composite is considered in this study with its mechanical and physical properties, including nonlinear shear, given in Table 1.

Thread contact in the joint is modeled as elastic contacts with a frictional (or frictionless) coefficient. Perfect bonding is assumed between composite plies in the tube body and at the interface between the composite lamina in the tube body and the threads in the joint region.

4.2 Governing Differential Equations

The strain-displacement relation in the composite is expressed as

$$\varepsilon = \frac{1}{2}(\nabla \mathbf{u} + \mathbf{u}\nabla) \tag{4-1}$$

where ε is the strain tensor and $\mathbf{u}$ is the displacement vector.

Each composite ply has transversely isotropic constitutive equations with shear nonlinearity, i.e.,

$$\varepsilon = \mathbf{S}(\sigma) : \sigma \tag{4-2}$$

The equilibrium equations are

$$\nabla \cdot \sigma = 0 \tag{4-3}$$

4.3 Thread Contact and Interface Conditions

Contact mechanics formulation is used in the study for thread surface modeling. The thread opening conditions are given as

$$\mathbf{n} \cdot \sigma = 0 \tag{4-4}$$

$$\mathbf{n} \cdot (\mathbf{u}^{(2)} - \mathbf{u}^{(1)}) > \delta_n \tag{4-5}$$

joint axis) by a factor of ξ=2 [where ξ is defined as the relative pin or box wall thickness] increases significantly the bearing pressure, whereas decreasing the pin section thickness reduces appreciably the thread bearing pressure. In a joint subject to combined pressure, axial, and makeup loading with a relatively high hoop-to-axial stress ratio, the critical bearing pressure on the first contacted thread of the thicker-box joint decreases more slowly with internal pressure than that in the reference (original) joint. On the other hand, the bearing pressure on the critical thread in the thinner-pin joint may even increase with internal pressure in pure internal pressure ($\lambda = 1/0$) and high hoop-to-axial (e.g. $\lambda = 4/1$) loading cases. Its thread bearing pressure decreases slowly with increasing internal pressure in the case of a low hoop-to-axial stress ratio (e.g. $\lambda = 2/1$). Therefore, the joint with a higher box-to-pin thickness ratio may have less adverse effect of internal pressure on the joint sealing. The jumps in Fig. 7-30 (b) indicate that damage occurs in the pin wall section, leading to a change in material stiffness and therefore a reduction in bearing pressure.

Failure and safe design envelopes for the joints with thicker box or thinner pin sections at T=2 are shown in Figs. (7-31)-(7-32). The joint with a thicker box provides a higher sealing capacity at a low axial-to-hoop stress ratio. But it is more prone to through-thickness damage in the pin section in the loading case with a high axial-to-hoop stress ratio. Similar to the thicker box case, the thinner-pin joint is more prone to through-thickness damage in the pin section in a stress state with a high axial-to-hoop ratio, whereas the sealing capacity of the joint under a loading with a low axial-to-hoop stress ratio has little improvement.

7.11 Effect of Thread Surface Friction

The influence of thread surface friction on the bearing pressure development on the first contacted thread in the original joint is studied. In the joint with a thread frictional coefficient 0.2, the results are shown in Fig. 7-33 for the λ=2:1 loading case with a two-turn makeup (T=2). The thread bearing pressure is found to increase slightly with increasing frictional coefficient.

7.12 Relationship Among Thread Bearing Pressure, Makeup Turns, and Applied Loading

The relationship among the thread bearing pressure, the applied internal pressure, the axial-to-hoop stress ratio, and the makeup turns is obtained in Fig. 7-34. Note that dP_B / dP_i is found to be a linear function of the axial-to-hoop stress ratio, and is independent of the makeup turns. Hence, linear regression is made on all the numerical results for T=1 and T=2 cases for further development of the relationship among the loading parameters and the thread bearing pressure.

The theoretical bearing pressure due to the makeup only can be calculated directly from the present analysis, as shown in Fig. 7-35. The bearing pressure in the joint under no external loading is found to increase proportionally with the makeup turns.

Based on all the aforementioned results, the following important engineering relationship among thread surface bearing pressure, external loading, and makeup turns may be established as

$$P_B = KT - (\alpha + \beta R)P_i \tag{7-1}$$

where P_B is the bearing pressure on a thread contact surface; T is the number of makeup turns; R=1/λ is the axial-to-hoop stress ratio; and K, α, β are coefficients, which can be determined once and for all for a given joint under any loading conditions.

Using the definitions of the threaded joint tightening factor of X and leakage safety factor S given in Section 5, one can determine the proper makeup for a threaded composite joint under a prescribed proportional external loading by

$$T = \frac{1}{K}[SX + (\alpha + \beta R)]P_i \tag{7-2}$$

where X is the threaded joint tightening factor, and S is the leakage safety factor.

The numerical results for K, α and β are obtained and shown in Table 2 for different joint designs considered in the study. The dependence of K, α and β on relative box wall thickness for the different design cases (relative to the original joint design) is shown in Figs. (7-36)-(7-38).

8. CONCLUSIONS

1) To understand the leakage failure resistance of a threaded composite joint and subsequently provide guidance on material and structural design of the composite joint, proper analytical modeling and carefully conducted experiments are required.

2) In this investigation, modifications and extension of a previously developed, nonlinear three-dimensional anisotropic mechanics model and an associated computational method have been made to study the leakage failure resistance of the threaded (SPH) composite joint under combined internal pressure, axial loading and makeup turns.

3) The composite mechanics method takes account of 3-D ply nonlinear constituent properties, different failure modes of individual composite plies, and progressive ply failure processes in the composite tube body.

4) The local thread deformation and failure are fully addressed by incorporating a nonlinear contact mechanics model and material failure criteria into the global joint analysis to determine localized bearing pressure distributions and stress concentrations along individual threads in the joint under general external loading.

5) The solution accuracy and validity of the predictive method are demonstrated by comparing carefully conducted tests and the analytical results for an 8-inch diameter SPH composite joint under combined internal pressure and makeup (turns) loading.

6) Leakage failure modes in the threaded composite joint have been analytically identified for various combinations of axial loading, internal pressure and makeup turns. Depending on the loading mode in the joint, the failure modes may include fiber- and matrix-dominated ply cracking in the tube body, thread material fracture, thread-pipe body interface debonding, and/or loss of bearing in the thread surface contact region.

7) Leakage due to initiation and growth of composite body damage through the wall thickness direction can be accurately predicted. The body-damage leakage mode is generally found in the joints containing a high level of axial stress. The critical axial stress in the joint (with a low hoop-to-axial-stress ratio) leading to the body-damage-mode leakage is not appreciably affected by makeup turns nor by the change in the hoop stress in the joint.

8) Leakage failure by loss of bearing pressure in the thread contact region can be accurately predicted by the analytically model and the associated computational mechanics method (as validated by test data.) The loss of bearing pressure in the threaded joints generally occurs in the cases with high hoop-to axial-stress ratios. In the SPH joint, increasing the makeup turns on the joint with a high hoop-to-axial stress-ratio significantly increases the leakage failure resistance of the joint.

9) Complete leakage failure maps (or envelopes) have been constructed analytically for the threaded SPH composite joints with nominal pin and box sections, thicker box sections, and thinner pin sections. Each leakage failure map generally contains three distinct regions: leakage, leak-prone, and leak-free regions, under different combinations of axial loading, internal pressure and makeup turns.

10) Each region in the threaded composite joint leakage failure map is governed by the failure criteria associated with distinct individual leakage failure mode, as identified in the analytical modeling/analysis.

11) Two important parameters, i.e., threaded-joint tightening factor and leakage safety factor, are introduced in the study for design, operation and reliability evaluation of individual composite joints. Based on the parameters (prescribed by joint performance requirements), safe design envelopes for reliable joint performance can be accurately constructed.

12) The effects of makeup turns and the external (pressure and axial) loading on the thread bearing pressure development have been determined in the SPH joint leakage study. In this joint, the influence by makeup turns and by the external loading on the loss of bearing pressure may be separable (and superimposable). A linear relationship is found among the thread bearing pressure, makeup turns and the internal pressure in the joint.

13) The bearing pressure on the critical thread in the SPH joint, i.e., the joint sealing capacity, is found to increase linearly with increasing makeup turns applied; however, the opposite is observed for the joints under combined external loading with high hoop-to-axial stress ratios. In these cases, the reduction in bearing pressure is at a rate nearly independent of the number of the makeup turns.

14) In the leakage analysis of the threaded SPH joints, an increase in the value of the frictional coefficient between the thread contact surface slightly raises the bearing pressure, and consequently, may improve the sealing capability of the joint, provided that the change in the frictional coefficient is not caused by altering the thread surface roughness.

15) For a given thread joint the coefficients, K, α and β, in the linear relationship among the makeup turns applied, internal pressure, axial loading, and the critical thread pressure can be determined once and for all for subsequent leakage resistance evaluation of the joint. Values of these coefficients have been determine for several cases, including the nominal SPH joint and SPH joints with different pin and box section thicknesses.

16) The threaded SPH joint with a thicker box section is found to possess a higher sealing capacity for the loading case with a low axial-to-hoop-stress ratio. But it is prone to the through-thickness-body damage in the pin section of the joint under a combined axial and pressure loading with a high axial-to-hoop stress ratio. The initial bearing

pressure due to pure makeup turns becomes larger with the thicker box wall, and the bearing pressure decreases slowly with increasing internal pressure loading.

17) The threaded SPH joint with a thin pin section is prone to through-thickness material damage in the pin section under the loading mode with a high axial-to-hoop-stress ratio. Its thread bearing pressure decreases slowly with increasing internal pressure in the case of a low hoop-to-axial stress ratio (e.g. $\lambda = 2/1$). In pure internal pressure ($\lambda = 1/0$) and high hoop-to-axial (e.g. $\lambda = 4/1$) loading cases, the thread bearing pressure may actually increase with the internal pressure. Also, the initial bearing pressure, due to pure makeup loading, is found to be small due to the compliance of the thin pin section.

9. REFERENCES

Bretl, J. L. and Cook, R. D. (1979). Modeling the load transfer in threaded connections by the finite element method. *International Journal for Numerical Methods in Engineering* **14**, 1359-1377.

Chiu, A. S. (1994). Test method for defining makeup procedure of fiberglass connections. *Appendix H of API Specification 15HR*, Second Draft.

Daniel, I. M. and Ishai, O. (1994). *Engineering Mechanics of Composite Materials.* Oxford University Press, New York.

Day, J. B., Moyer, M. C., and Hirshberg, A. J. (1989). New makeup method for API connections. In: *Proceedings of 1989 Drill Conference*, pp. 635-642.

Den Hartog, J. P. (1929). The mechanics of plate rotors for turbo generators. *Transaction of ASME* **51**, APM 51-1.

Dilintas, G. (1991). Investigation of a composite tubing connection performance. *Journal of Energy Resources Technology* **113**, 40-48.

Dilintas, G. (1992). Influence of the filament on the performance of a composite tubing connection. *Journal of Composite Materials* **26**, 1443-1454.

Dragoni E. (1992). Effect of thread pitch and frictional coefficient on the stress concentration in metric nut-bolt connections. In: *Proceedings of the 11th International Conference on Offshore Mechanics and Arctic Engineering*, edited by M. M. Salama, et al., ASME, New York, pp. 355-362.

Friedrich, R., Nyberg, P., and Francis, B. (2001). Investigation of joint leakage: Centron SPH threaded joints. Technical Report, Ameron International, South Gate, CA, February 2001.

Hahn, H. T. and Tsai, S. W. (1973). Nonlinear elastic behavior of unidirectional composite laminae. *Journal of Composite Materials* **7**, 102-118.

Hilbert, L. B. and Kalil, I. A. (1992). Evaluation of premium threaded connections using finite element analysis and full-scale testing. In: *Proceedings of Drilling Conference*, pp.562-580.

Jones, R., Sawyer, J. P. G. and Chiu, W. K. (1999). Studies in the matrix dominated failures of composite joints. *Composite Structures* **44**, 1-16.

Macdonald, K. A. and Deans, W. F. (1995). Stress analysis of drillstring threaded connections using the finite element method. *Engineering Failure Analysis* **2**, 1-30.

Rhee, H. C. (1990). Three-dimensional finite element analysis of threaded joints. In: *Proceedings of the 9th International Conference on Offshore Mechanics and Arctic Engineering*, pp. 293-298.

Sun, Hsien-Tang, Yan, Yanmin, and Chang, Fu-Kuo (1997). Lateral constraining effect on bolted composite joints. *AIAA/ASME/ASCE/AHS/ASC Structures, Structural Dynamics & Materials Conference*, Vol. **3**, pp. 2010-2020.

Swanson, S. R., Messick, M. J., and Tian, Z. (1987). Failure of carbon/epoxy lamina under combined stress. *Journal of Composite Materials* **21**, 619-630.

Wang, S. S. and Lu, X. (1996). Leakage failure of threaded fiber-composite joints under combined internal pressure, axial and makeup loading: experiments and analysis. *CEAC-TR*-96-0102.

Wang, S. S. and Srinivasan, S. (1996). Long-term leakage failure of filament-wound fiberglass composite laminate tubing under combined internal pressure and axial loading. *CEAC-TR*-96-0101.

Weiner P. D. and Swell, F. D. (1967). New technology for improved tubular connection performance. *Journal of Petroleum Technology* **19**, 227-343.

10. TABLES

Table 1. Mechanical properties of filament-wound glass/epoxy composite

E_{11} (Msi)	E_{22} (Msi)	ν_{12}	ν_{23}	G_{12} (Msi)	S_{6666} $(psi)^{-3}$	X_1^+ (Ksi)	X_1^- (Ksi)	X_2^+ (Ksi)	X_2^- (Ksi)	X_6 (Ksi)
7.0	1.9	0.313	0.313	0.83	1.65E-14	110	100	6.86	-22.00	10.60

Table 2. Dependence of K, α and β on relative box and pin wall thicknesses

Thickness	K (Ksi/turn)	α	β
1.0	1.391	0.720	1.672
1.5 (box)	1.508	0.413	1.875
2.0 (box)	1.566	0.236	2.160
2.5 (box)	1.600	0.217	3.803
0.5 (pin)	0.589	-0.464	1.206

11. FIGURES

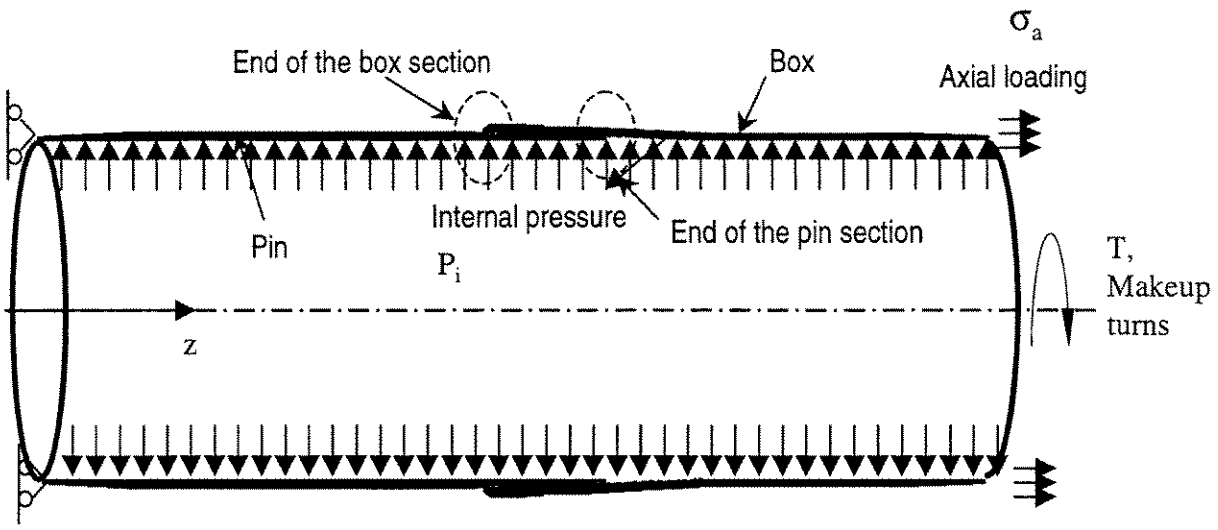

4.1 (a) Global Joint Geometry and Loading.

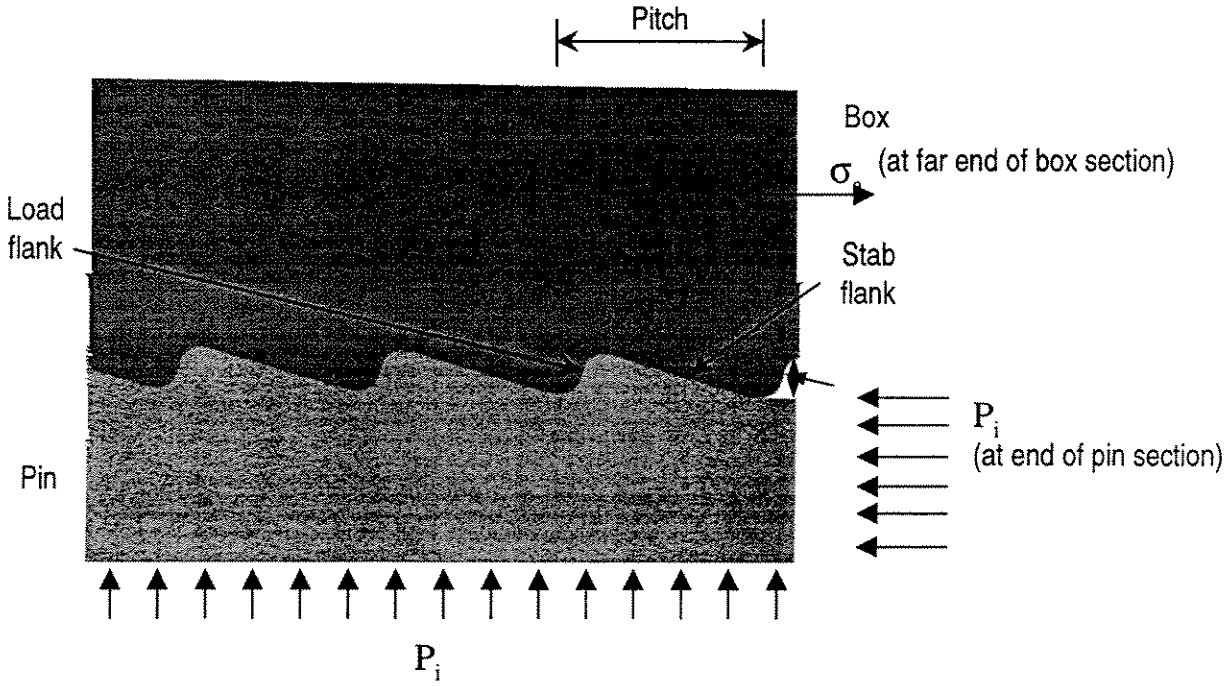

Fig.4-1 (b) Local Thread Profile in Composite Joint.

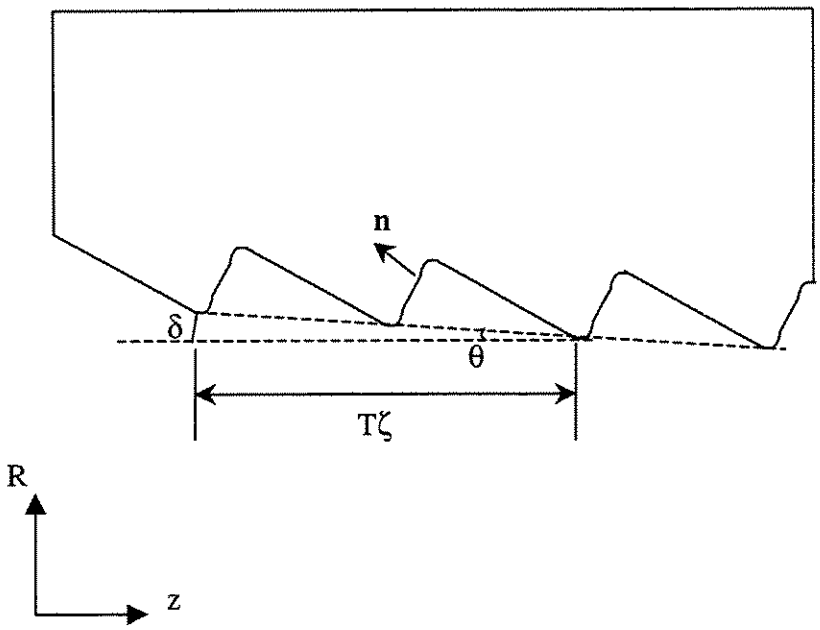

Fig.4-2 Local Geometric Parameters in Composite Joint.

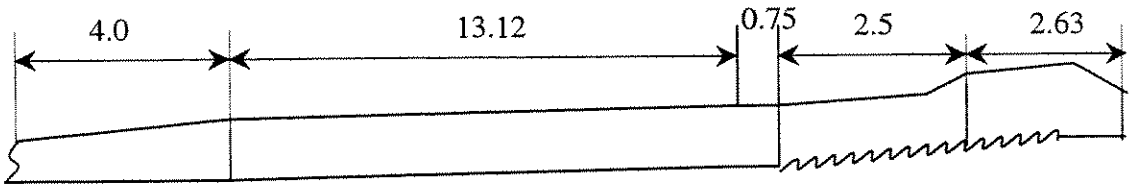

(a)

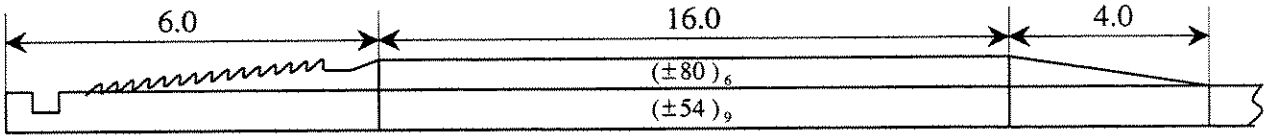

(b)

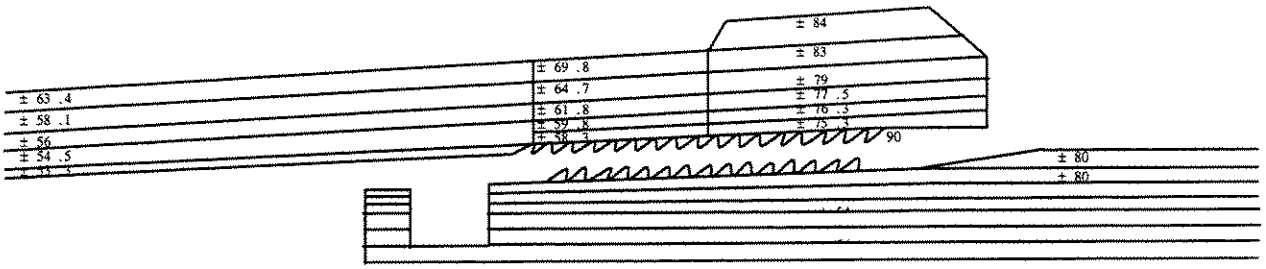

(c)

Fig.7-1 Geometric Modeling of a Threaded Composite Joint;

(a) Box Section, (b) Pin Section, and (c) Composite Joint.

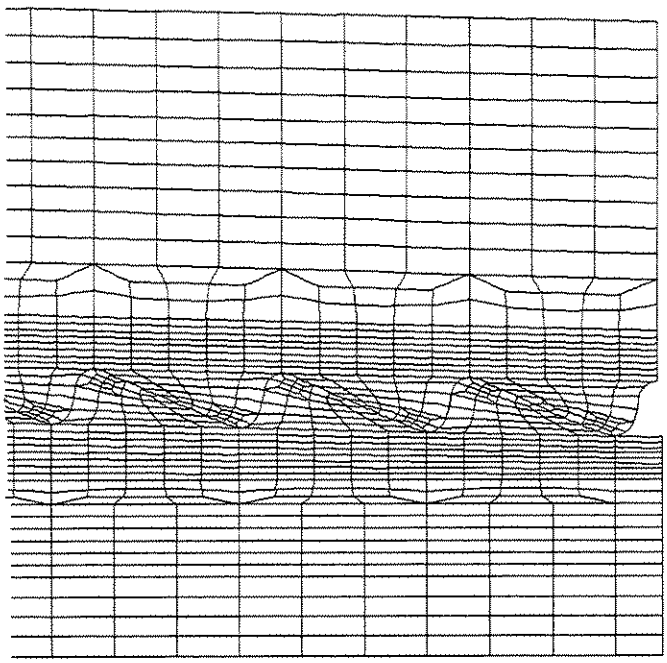

Fig.7-2 Typical Finite Element Discretization for Modeling Local Thread Contact.

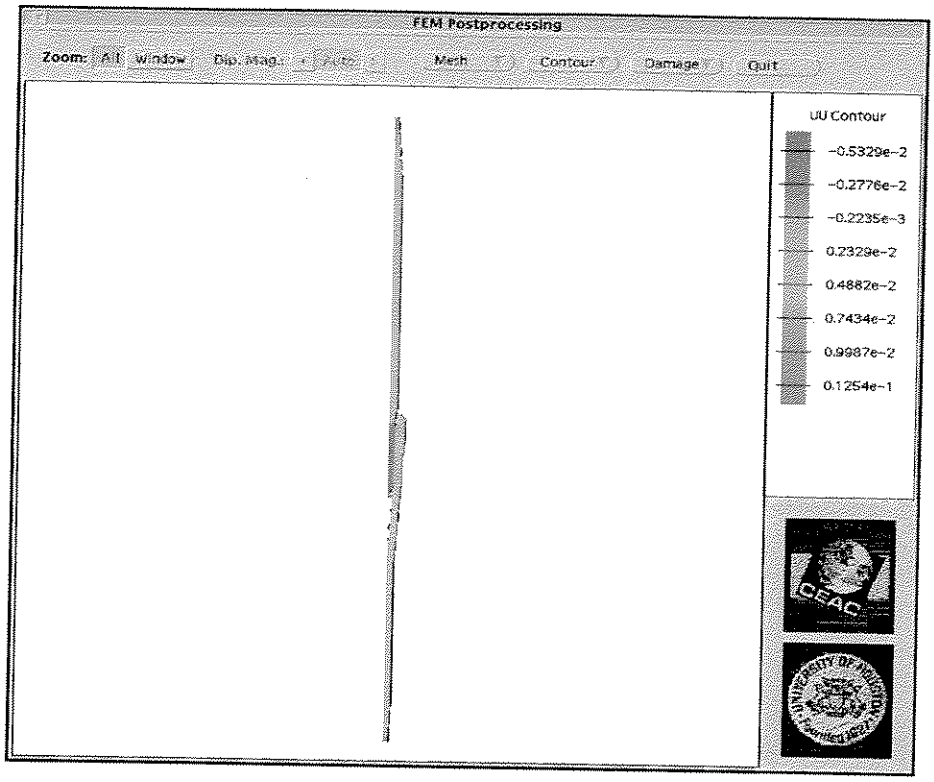

Fig. 7-3 Radial Displacement of the Joint of Original Design at Internal Pressure 0.804 Ksi and Axial Tension 6 Ksi (λ=2:1) at T=2.

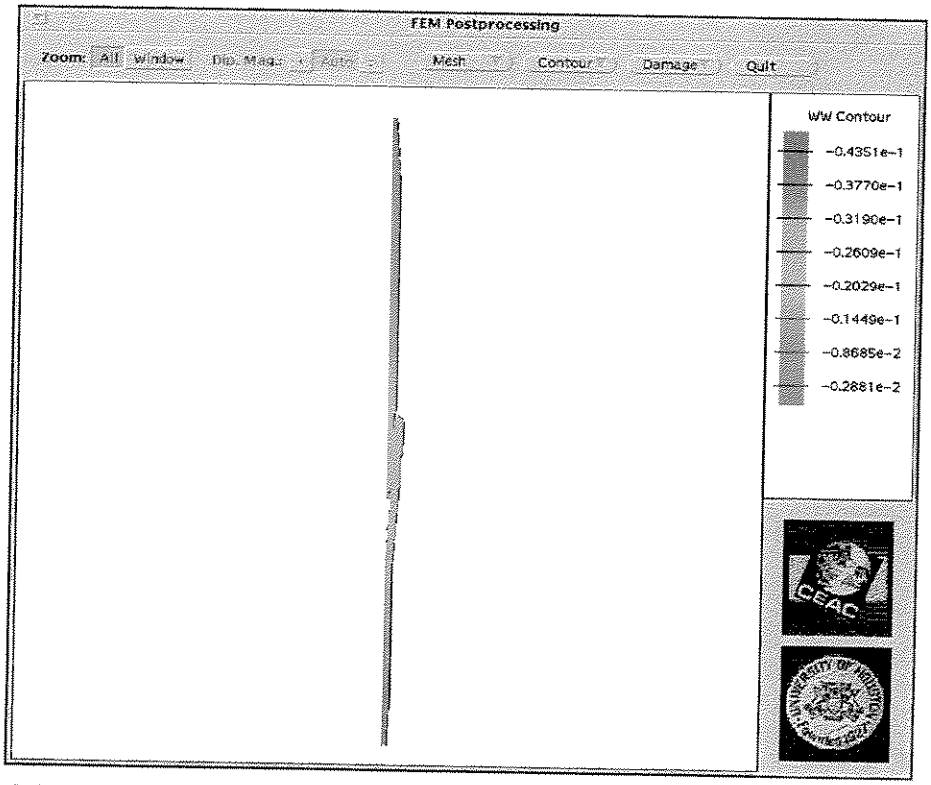

Fig. 7-4 Axial Displacement of the Joint of Original Design at Internal Pressure 0.804 Ksi and Axial Tension 6 Ksi (λ= 2:1) at T=2.

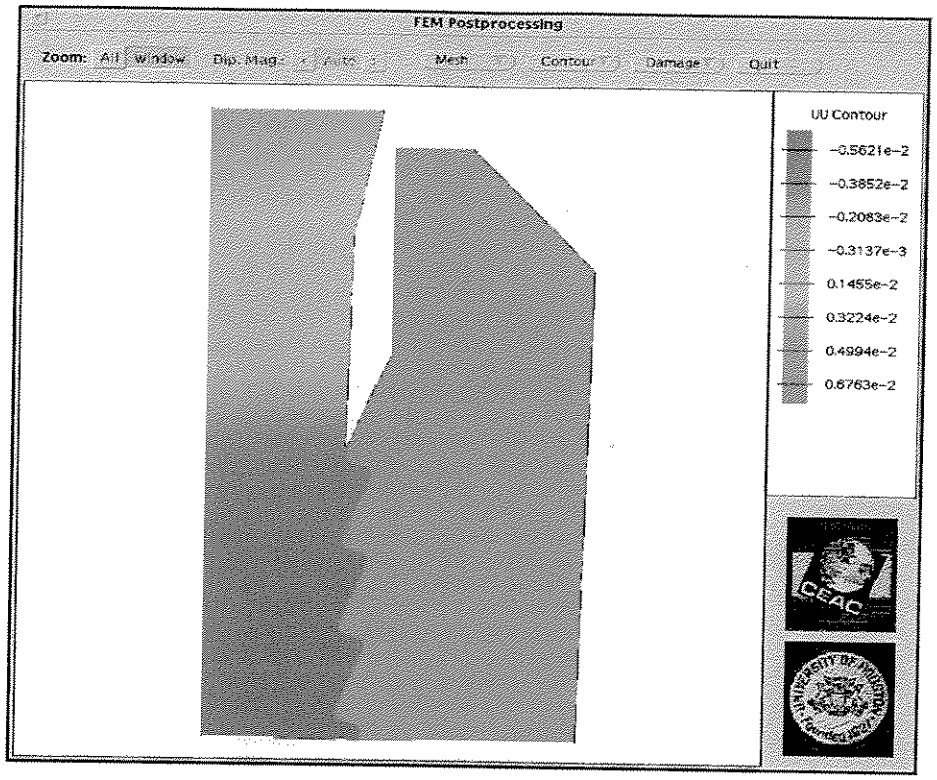

Fig. 7-5 Radial Displacement Distribution Near the End of Box Section of a Threaded Joint at Internal Pressure 0.804 Ksi and Axial Tension 6 Ksi (λ= 2:1) at T=2.

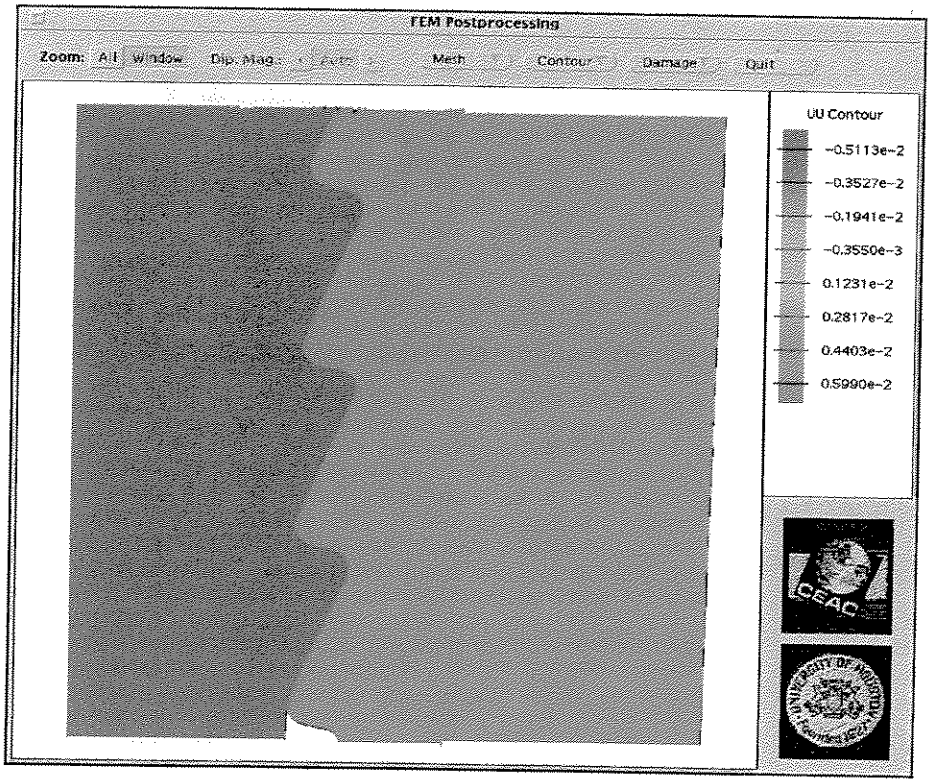

Fig. 7-6 Radial Displacement Distribution Near the End of Pin Section of a Threaded Joint at Internal Pressure 0.804 Ksi and Axial Tension 6 Ksi (λ= 2:1) at T=2.

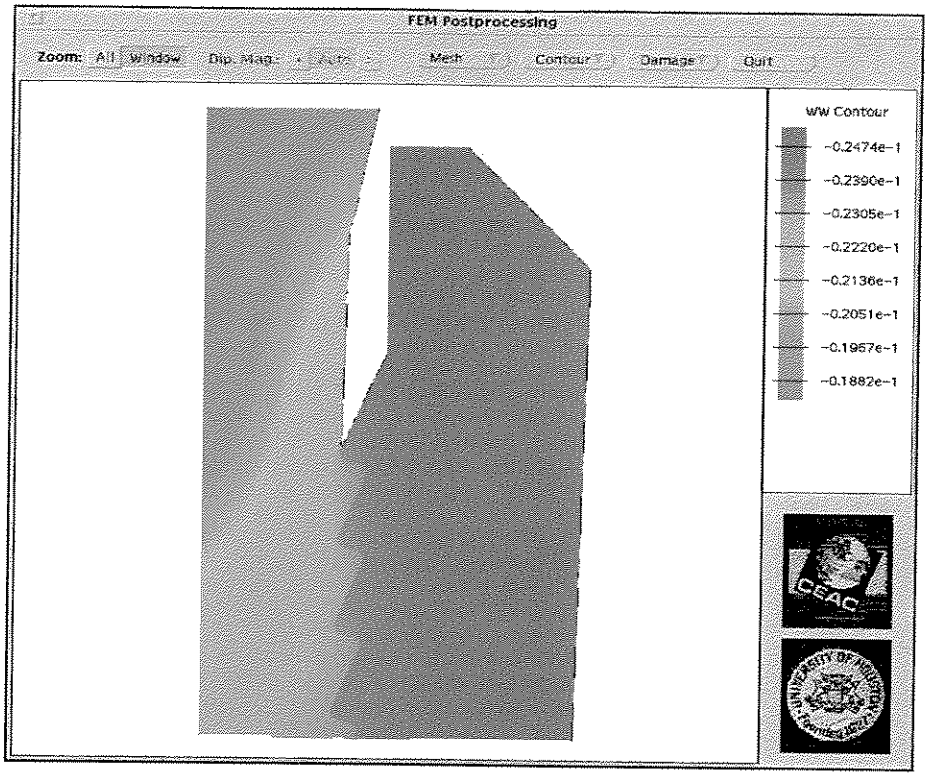

Fig. 7-7 Axial Displacement Distribution Near the End of Box Section of a Threaded Joint at Internal Pressure 0.804 Ksi and Axial Tension 6 Ksi (λ= 2:1) at T=2.

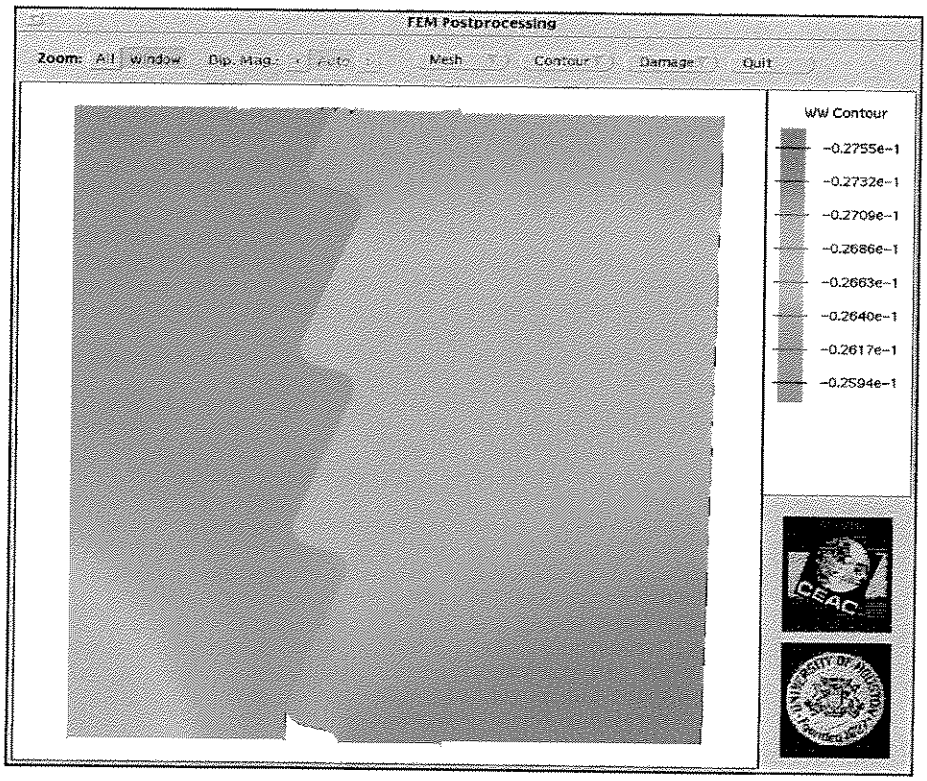

Fig. 7-8 Axial Displacement Distribution Near the End of Pin Section of a Threaded Joint at Internal Pressure 0.804 Ksi and Axial Tension 6 Ksi (λ= 2:1) at T=2.

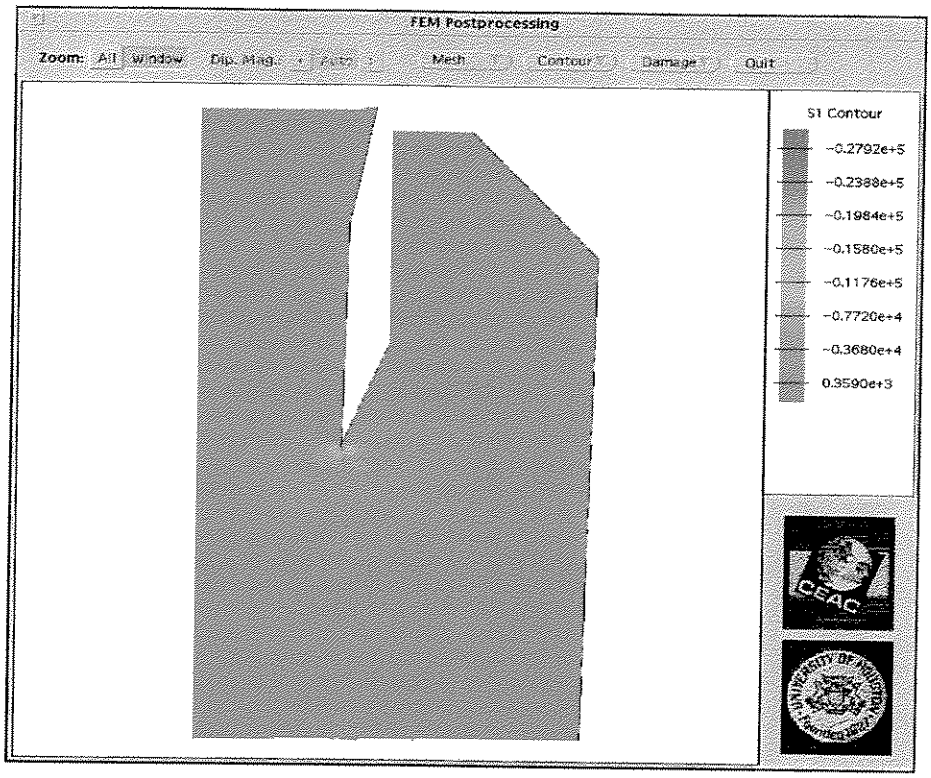

Fig. 7-9 Interlaminar Normal Stress σ_R Near the End of Box Section of a Threaded Joint at Internal Pressure 0.804 Ksi and Axial Tension 6 Ksi (λ= 2:1) at T=2.

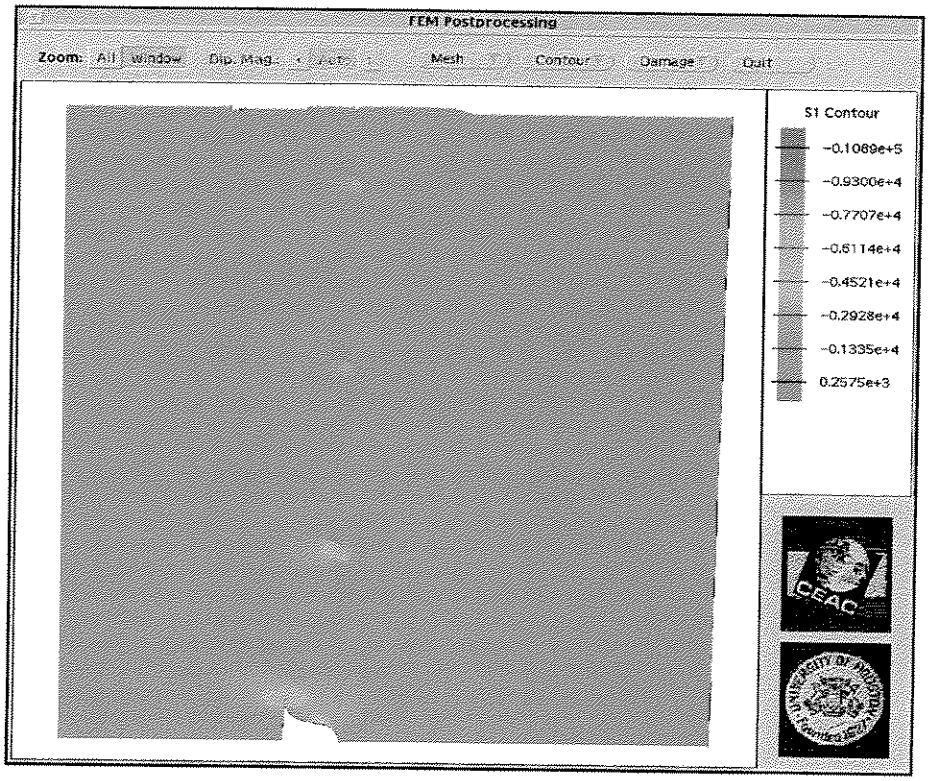

Fig. 7-10 Interlaminar Normal Stress σ_R Near the End of Pin Section of a Threaded Joint at Internal Pressure 0.804 Ksi and Axial Tension 6 Ksi (λ= 2:1) at T=2.

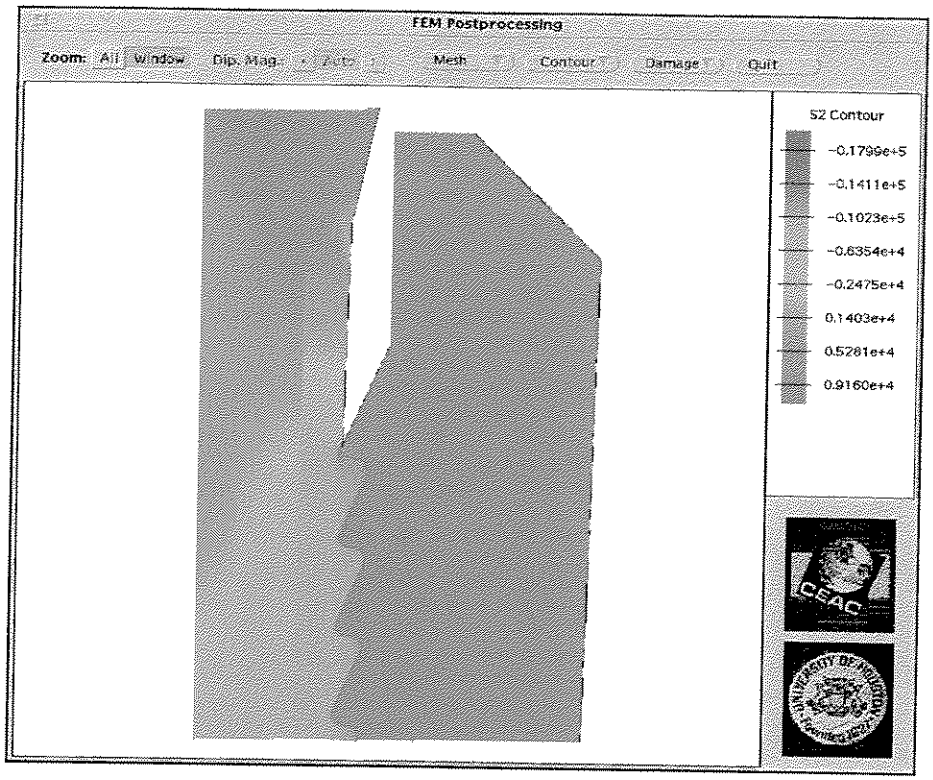

Fig. 7-11 Circumferential Stress σ_θ Near the End of Box Section of a Threaded Joint at Internal Pressure 0.804 Ksi and Axial Tension 6 Ksi (λ= 2:1) at T=2.

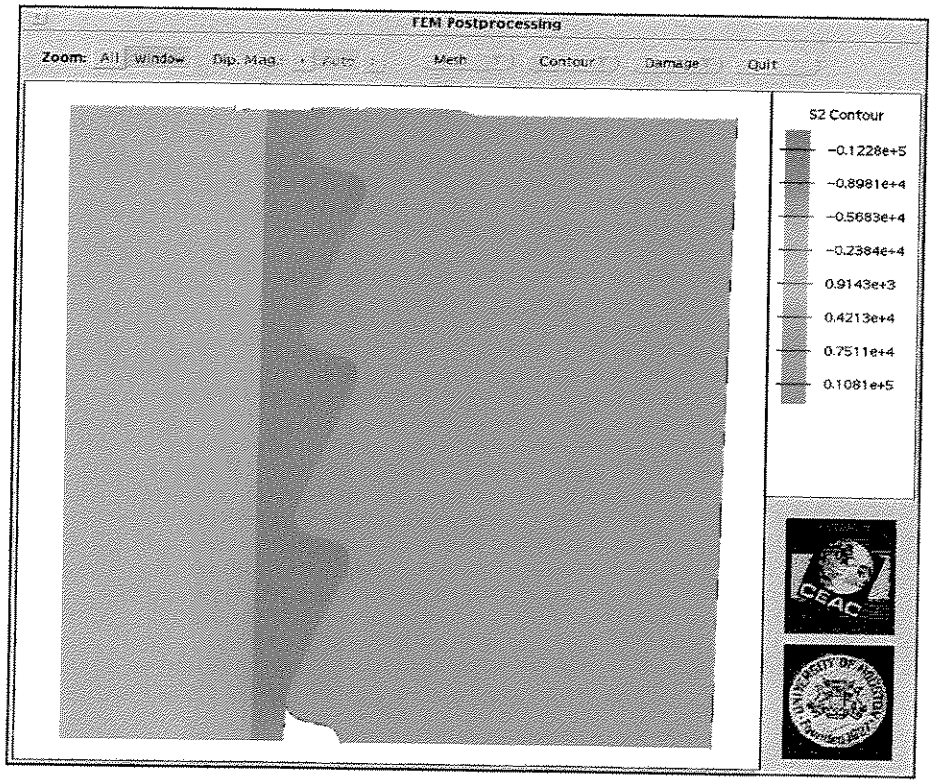

Fig. 7-12 Circumferential Stress σ_θ Near the End of Pin Section of a Threaded Joint at Internal Pressure 0.804 Ksi and Axial Tension 6 Ksi (λ= 2:1) at T=2.

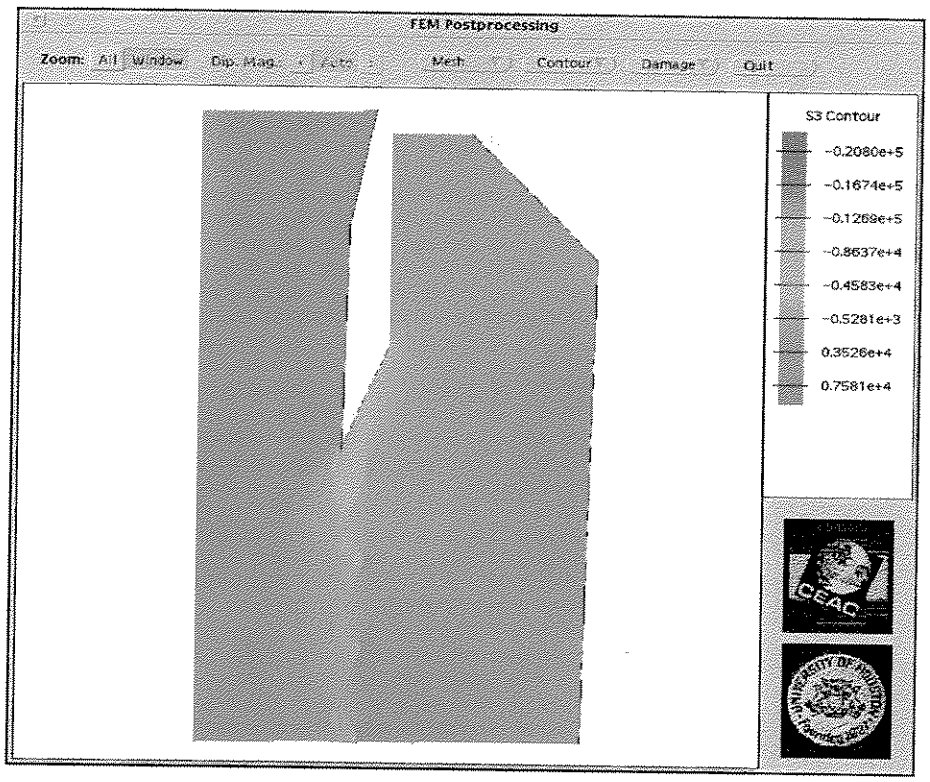

Fig. 7-13 Axial Stress σ_Z Near the End of Box Section of a Threaded Joint at Internal Pressure 0.804 Ksi and Axial Tension 6 Ksi (λ= 2:1) at T=2.

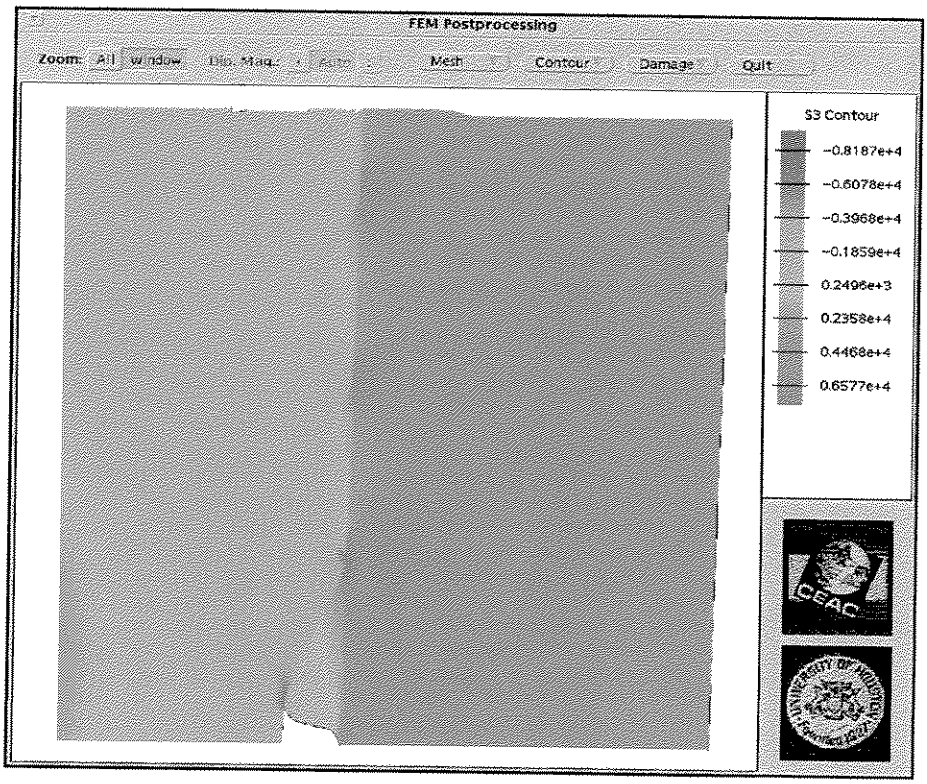

Fig. 7-14 Axial Stress σ_Z Near the End of Pin Section of a Threaded Joint at Internal Pressure 0.804 Ksi and Axial Tension 6 Ksi (λ= 2:1) at T=2.

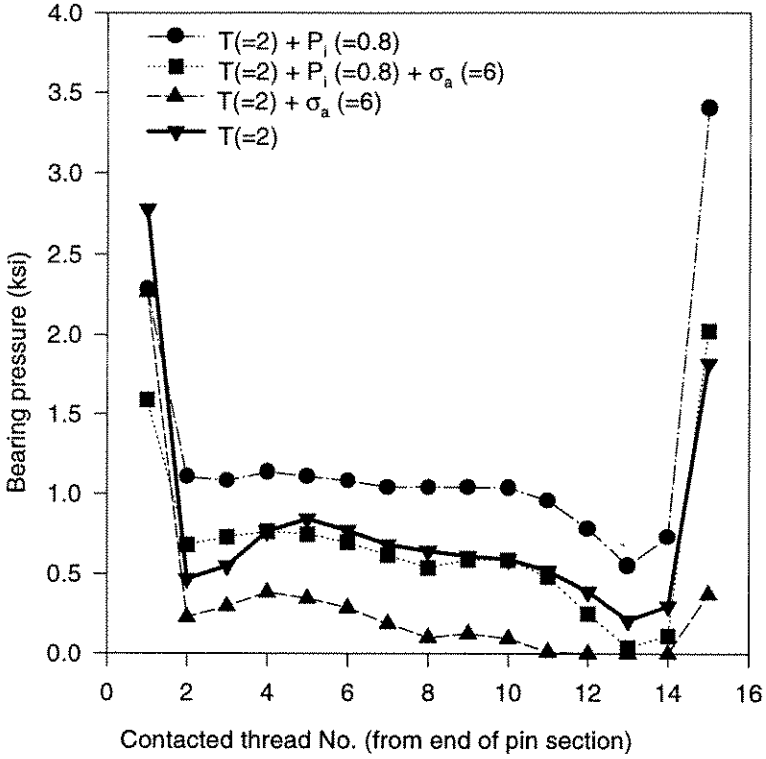

Fig. 7-21 Thread Bearing Pressure P_B at Stab Flank of Contact Threads in a Joint Subject to Several Different Loading Cases (T=2).

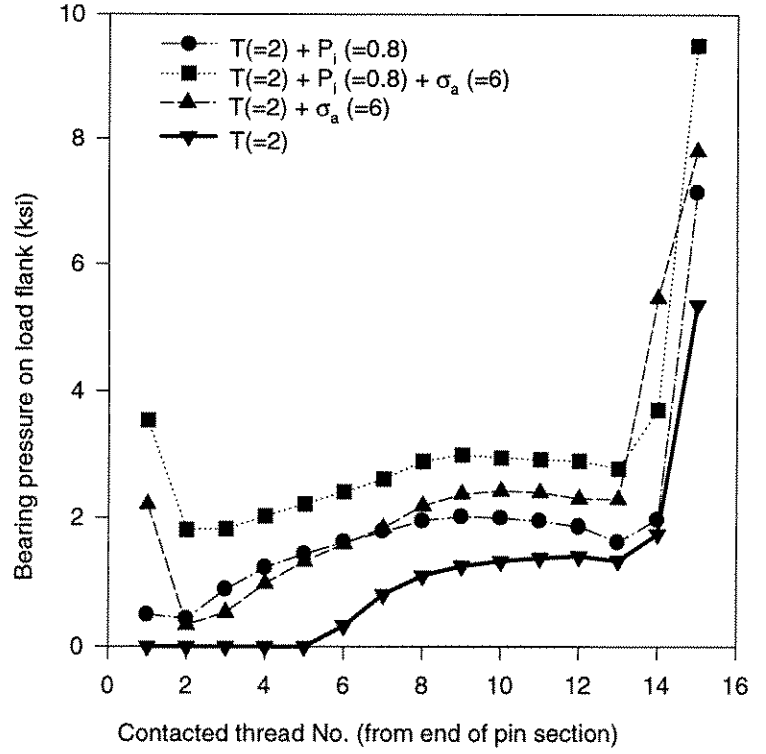

Fig. 7-22 Bearing Pressure at Load Flank of Contact Threads in a Joint Subject to Several Different Loading Cases (T=2).

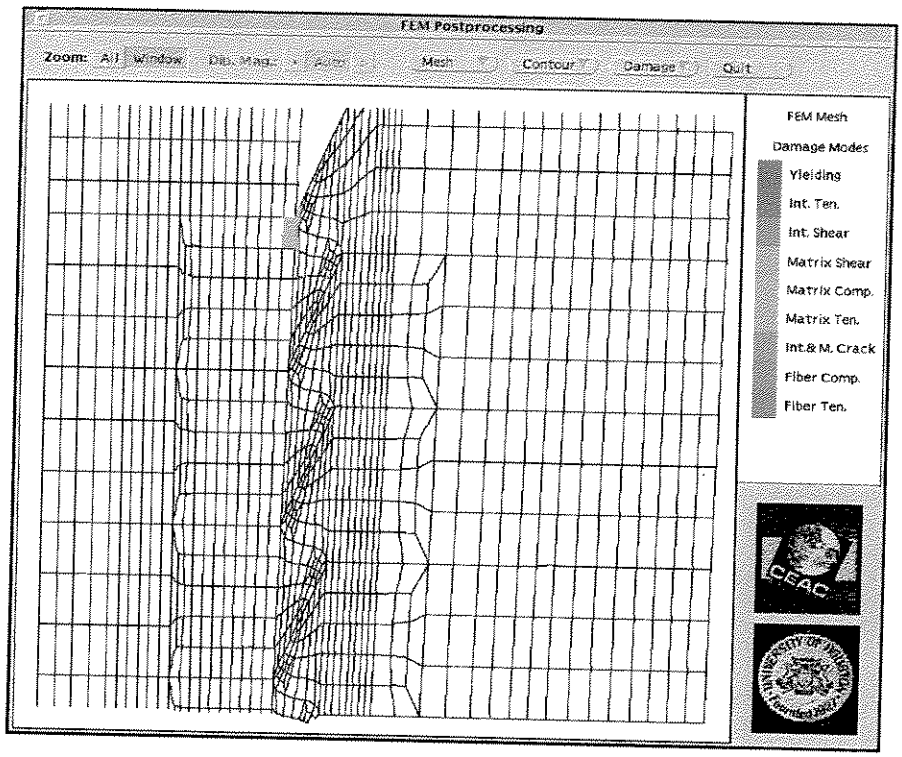

Fig. 7-23 Damage Modes and Progressive Growth in a Threaded Joint Under Pure Internal Pressure 1.6 Ksi at T=2 (Just After Loss of Bearing Pressure).

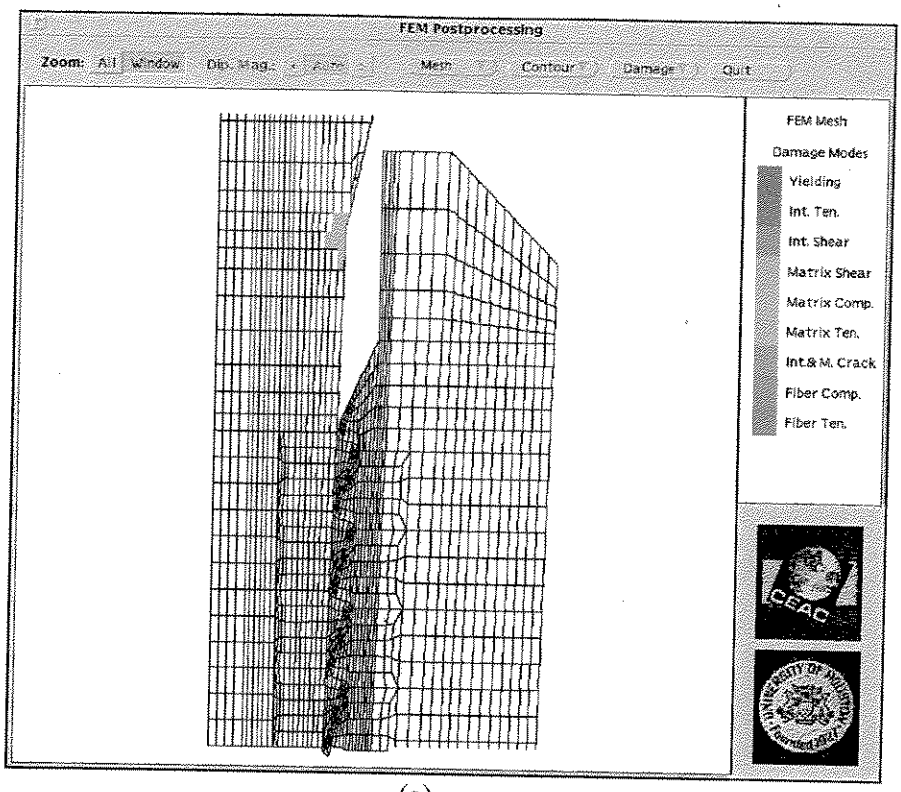
FEM Postprocessing
Zoom: All Window
Mesh
Contour
Damage
Quit
FEM Mesh
Damage Modes
Yielding
Int. Ten.
Int. Shear
Matrix Shear
Matrix Comp.
Matrix Ten.
Int.& M. Crack
Fiber Comp.
Fiber Ten.
CEAC

(a)

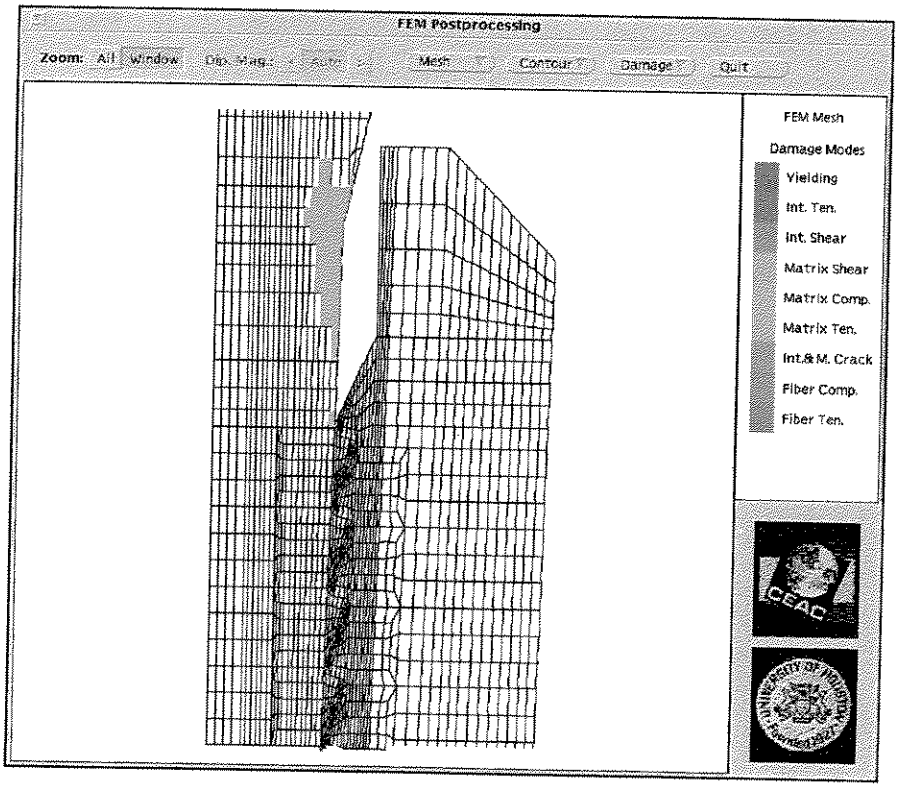
FEM Postprocessing
Zoom: All Window
Mesh
Contour
Damage
Quit
FEM Mesh
Damage Modes
Yielding
Int. Ten.
Int. Shear
Matrix Shear
Matrix Comp.
Matrix Ten.
Int.& M. Crack
Fiber Comp.
Fiber Ten.
CEAC

(b)

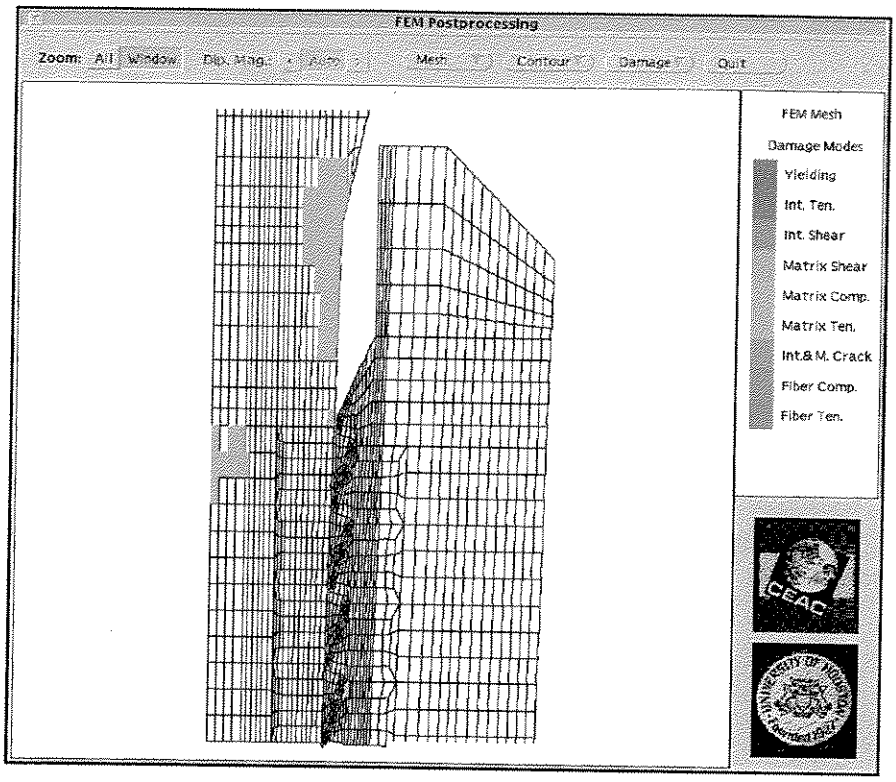

(c)

Fig. 7-24 Damage Modes and Growth Near the End of Box Section Under Combined Internal Pressure and Axial Tension (λ=2:1) at T=2.
(a) P_i=0.80 Ksi and σ_a=6 Ksi; (b) P_i=1.07 Ksi and σ_a=8 Ksi;
(c) P_i= 1.14 Ksi and σ_a=8.5 Ksi.

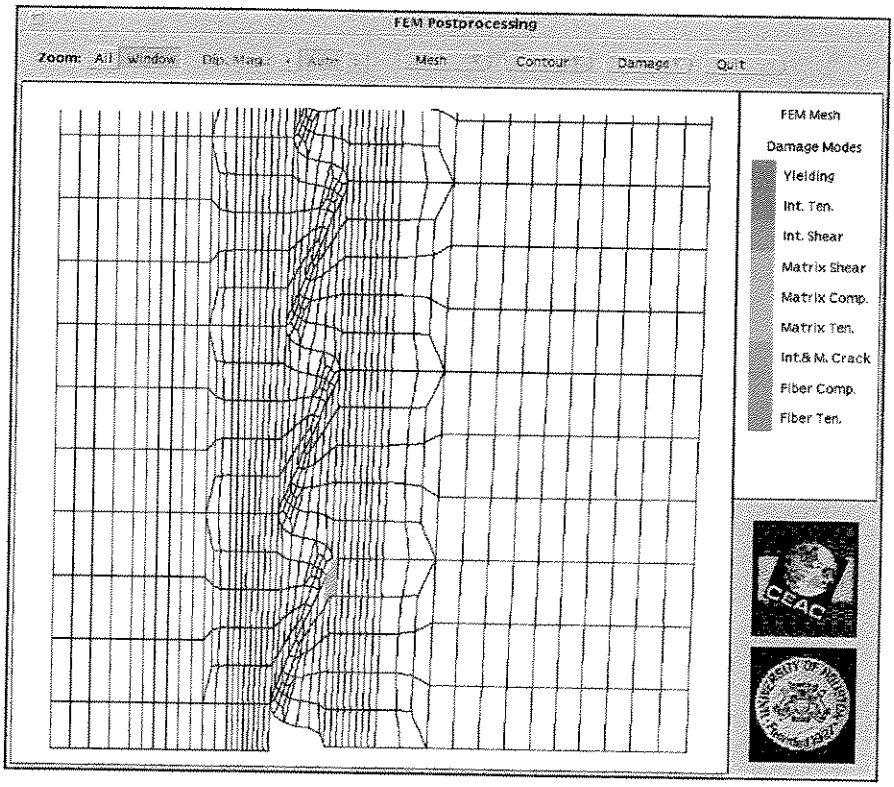

(a)

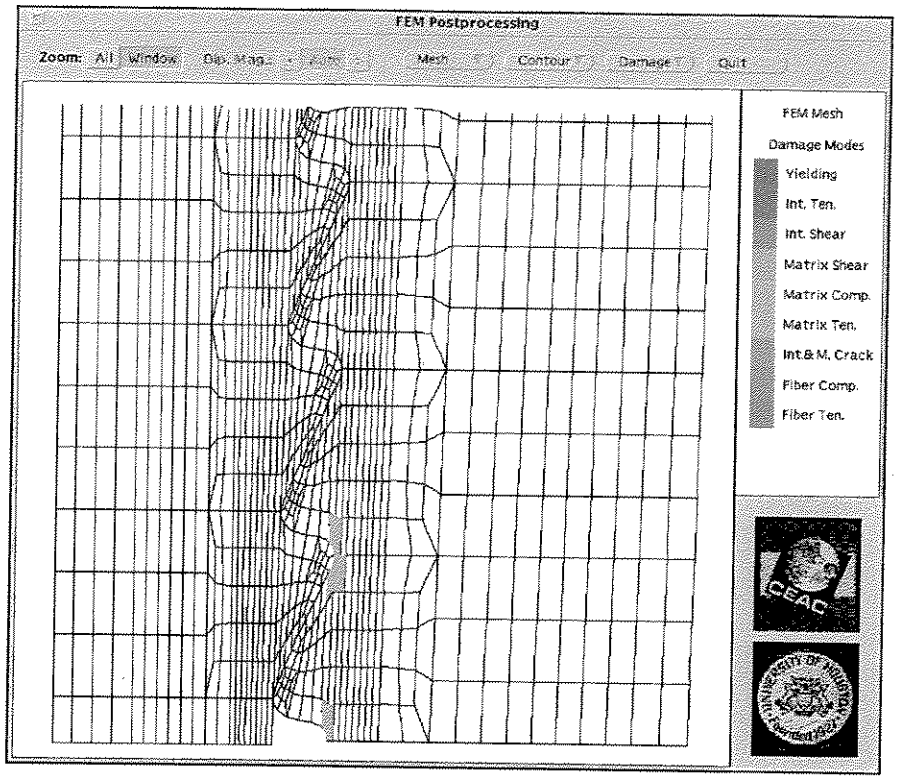

(b)

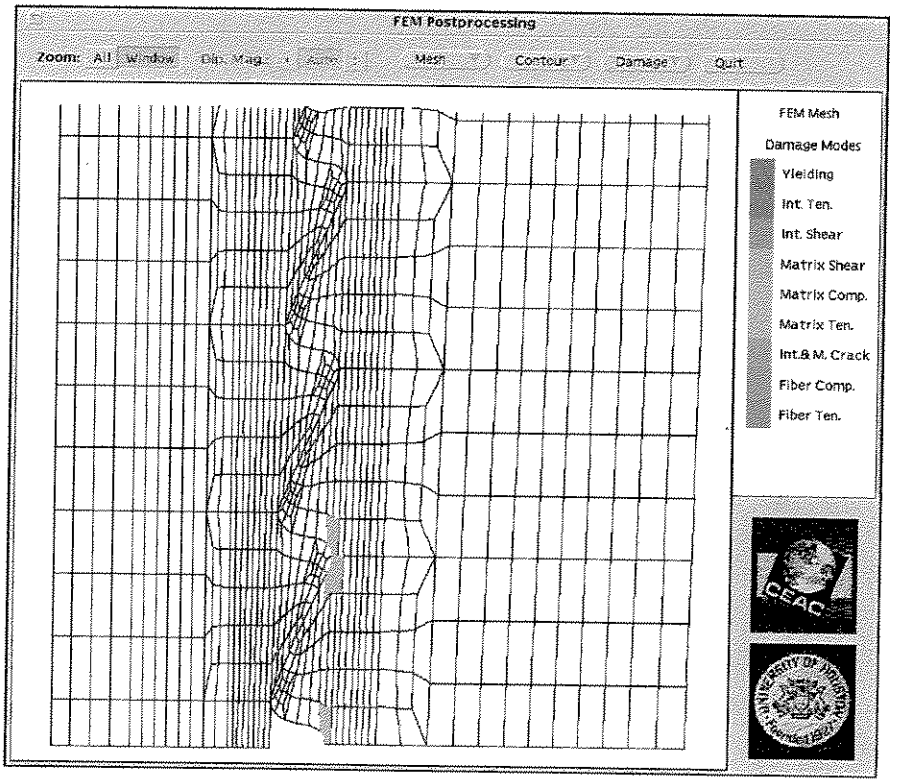

(c)

Fig. 7-25 Damage Modes and Growth Near the End of Pin Section Under Combined Internal Pressure and Axial Tension (λ=2:1) at T=2.
(a) P_i=0.80 Ksi and σ_a=6 Ksi; (b) P_i=1.07 Ksi and σ_a=8 Ksi;
(c) P_i= 1.14 Ksi and σ_a=8.5 Ksi.

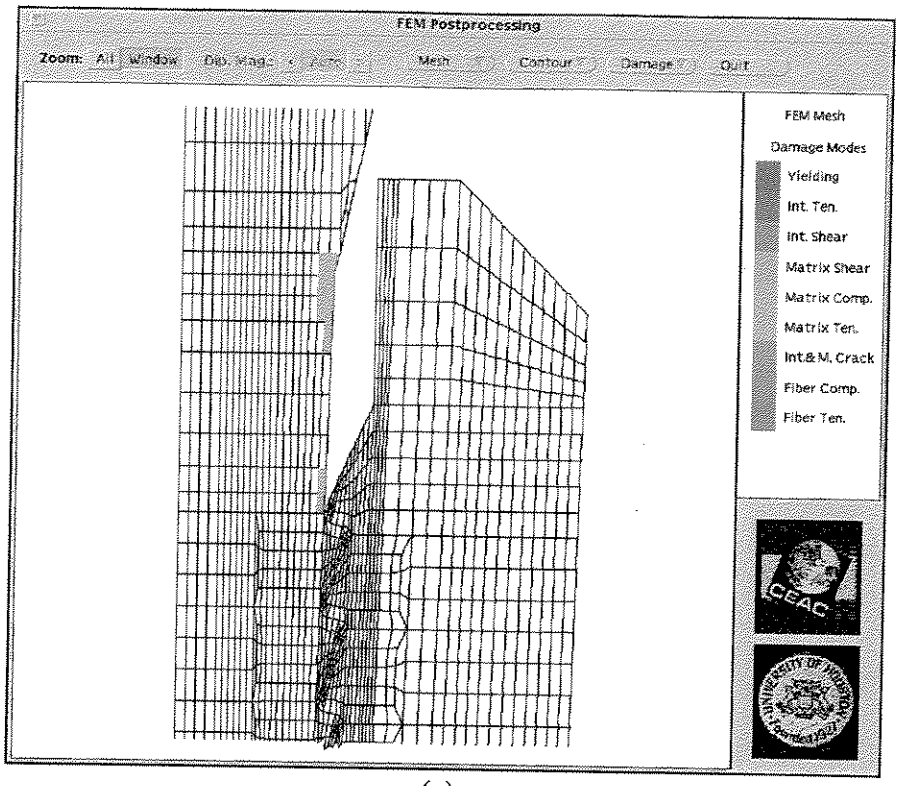
FEM Postprocessing
Zoom: All Window
Mesh
Contour
Damage
Quit
FEM Mesh
Damage Modes
Yielding
Int. Ten.
Int. Shear
Matrix Shear
Matrix Comp.
Matrix Ten.
Int.& M. Crack
Fiber Comp.
Fiber Ten.
CEAC

(a)

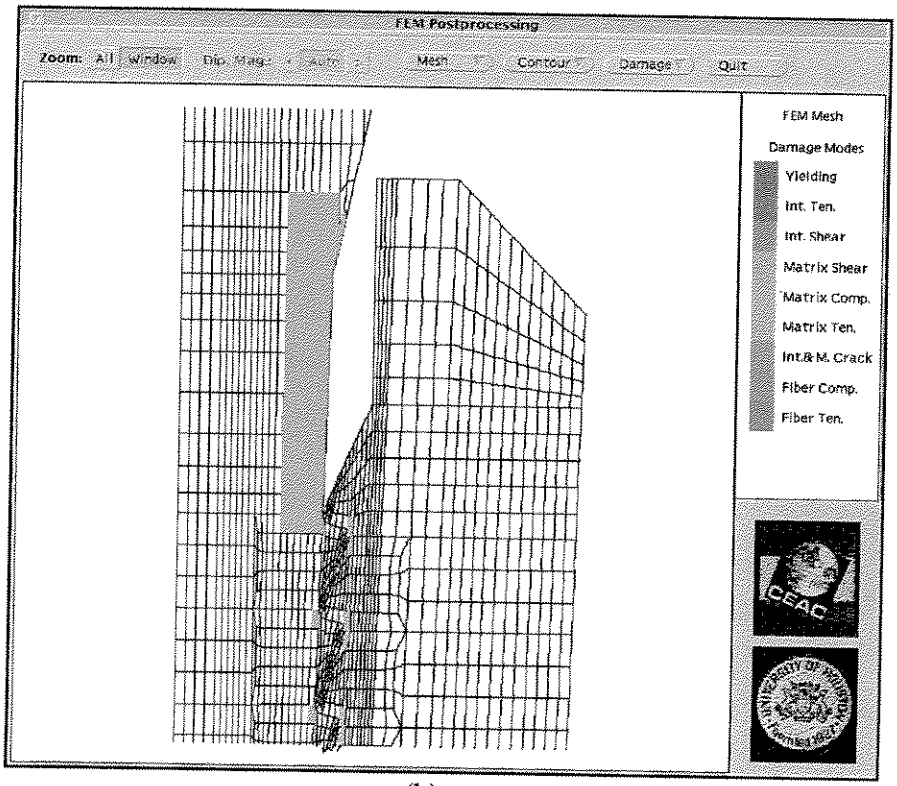
FEM Postprocessing
Zoom: All Window
Mesh
Contour
Damage
Quit
FEM Mesh
Damage Modes
Yielding
Int. Ten.
Int. Shear
Matrix Shear
Matrix Comp.
Matrix Ten.
Int.& M. Crack
Fiber Comp.
Fiber Ten.
CEAC

(b)

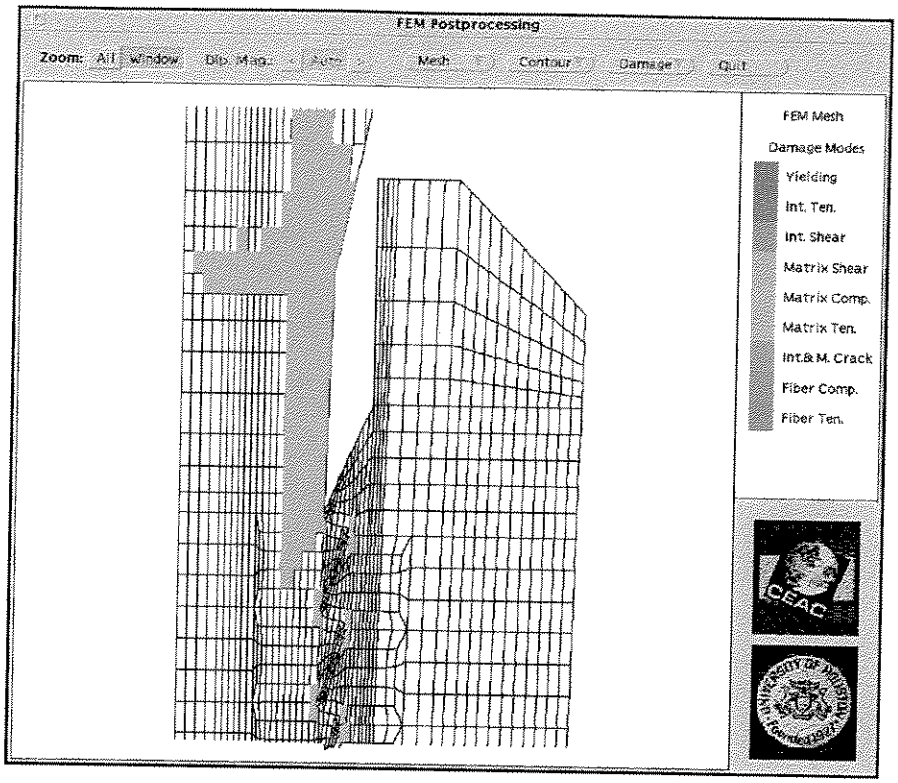

(c)

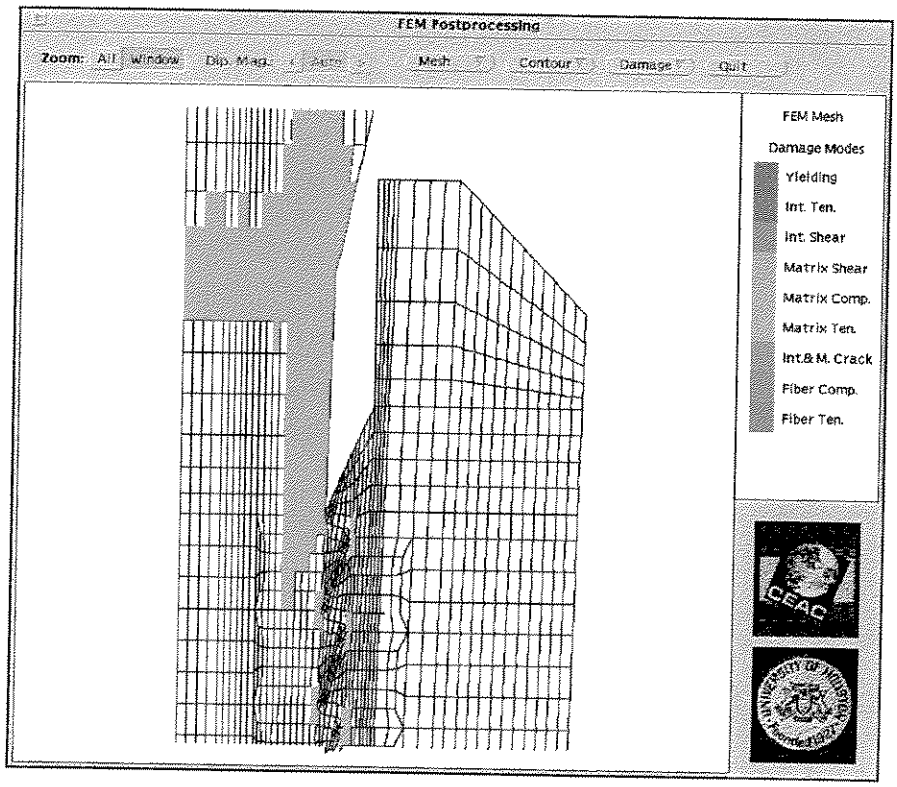

(d)

Fig.7-26 Damage Modes and Growth Near the End of Box Section Using Three-Region Failure Criterion Under Axial Tension (T=2).
(a) σ_a=7 Ksi; (b) σ_a=11 Ksi; (c) σ_a=13.5 Ksi; (d) σ_a=14 Ksi.

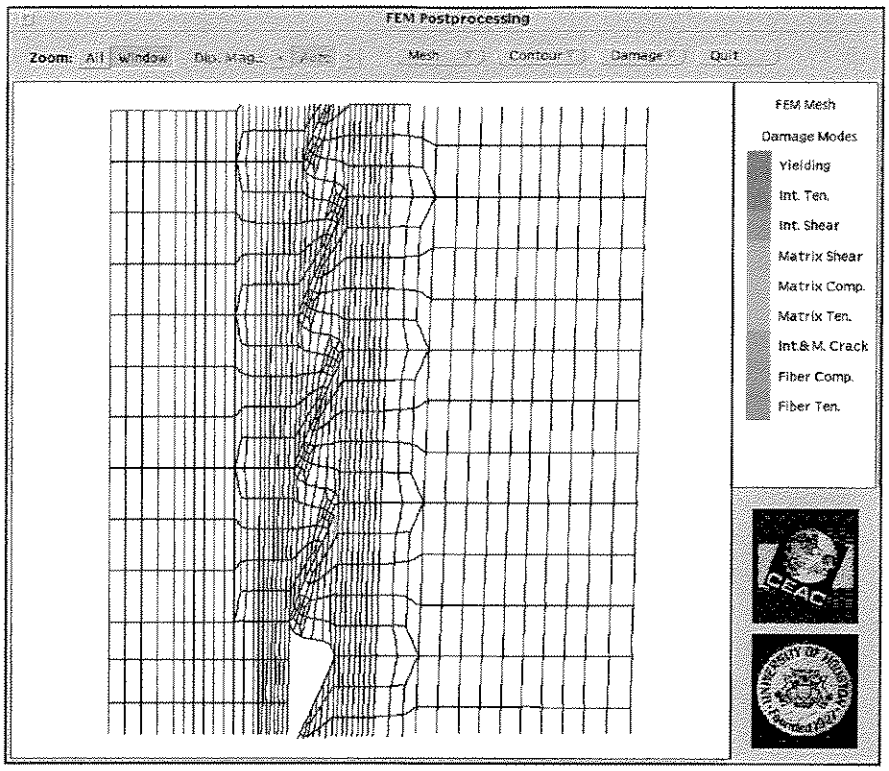
FEM Postprocessing
Zoom: All Window
Mesh
Contour
Damage
Quit
FEM Mesh
Damage Modes
Yielding
Int. Ten.
Int. Shear
Matrix Shear
Matrix Comp.
Matrix Ten.
Int.&M. Crack
Fiber Comp.
Fiber Ten.
CEAC

(a)

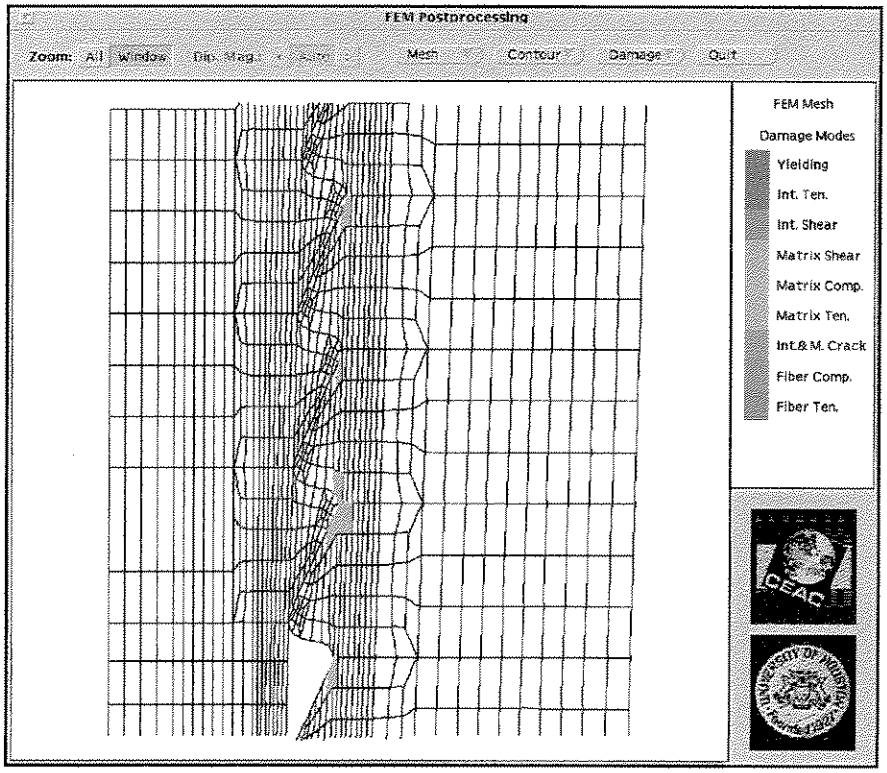
FEM Postprocessing
Zoom: All Window
Mesh
Contour
Damage
Quit
FEM Mesh
Damage Modes
Yielding
Int. Ten.
Int. Shear
Matrix Shear
Matrix Comp.
Matrix Ten.
Int.&M. Crack
Fiber Comp.
Fiber Ten.
CEAC

(b)

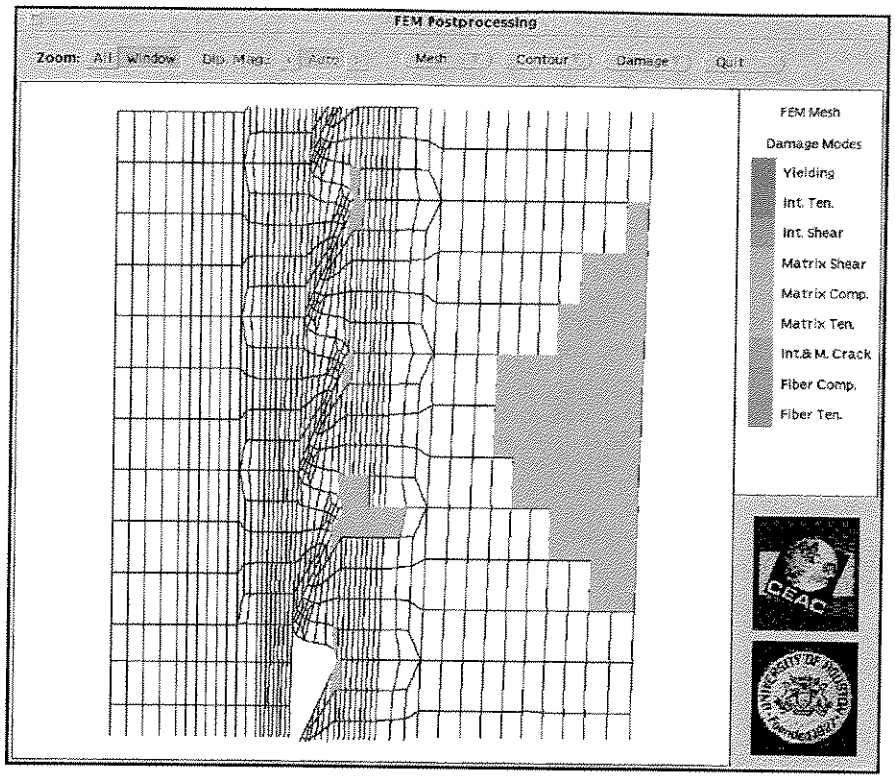

(c)

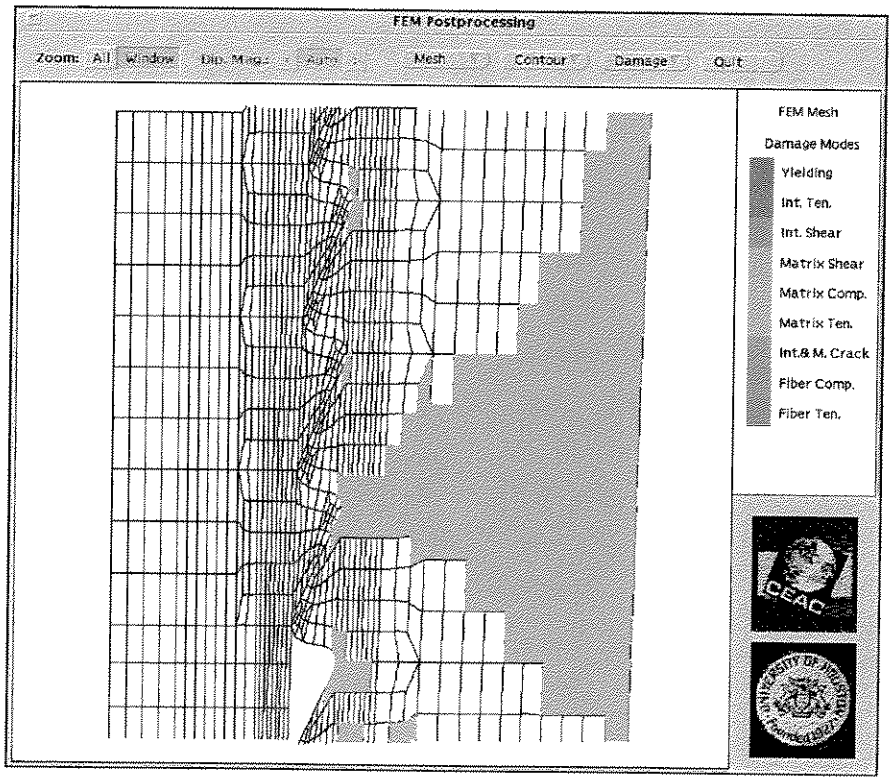

(d)

Fig.7-27 Damage Modes and Growth Near the End of Pin Section Using Three-Region Failure Criterion Under Axial Tension (T=2).
(a) σ_a=7 Ksi; (b) σ_a=11 Ksi; (c) σ_a=13.5 Ksi; (d) σ_a=14 Ksi.

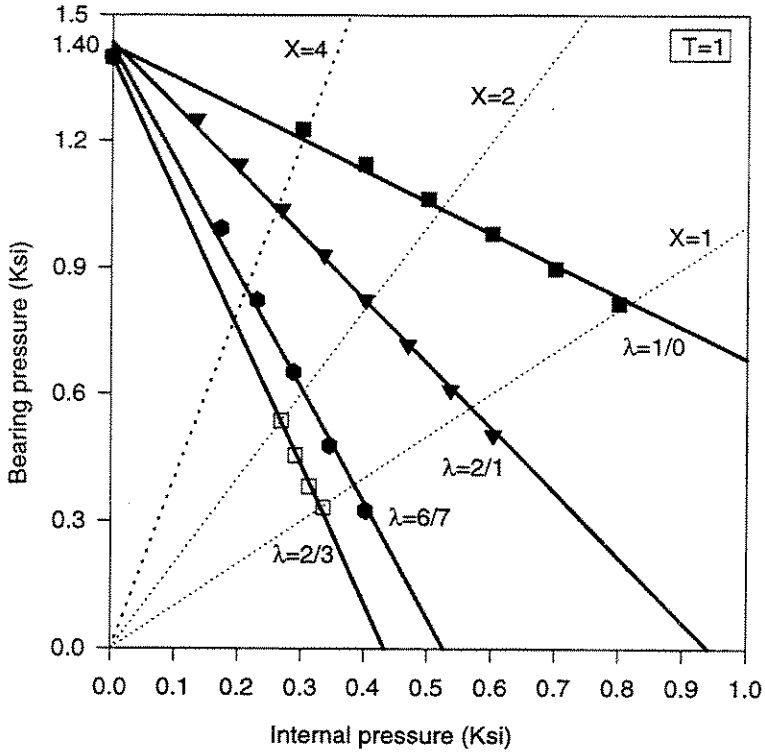

(a)

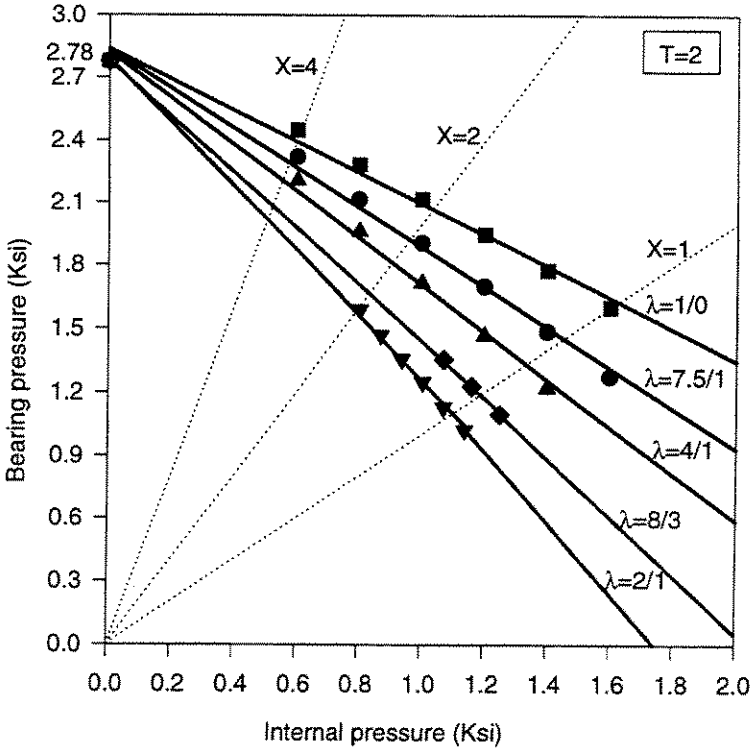

(b)

Fig. 7-28 Effect of Internal Pressure and Makeup Turn on Thread Bearing Pressure Development in a Threaded Composite Joint with: (a) T=1; (b) T=2.

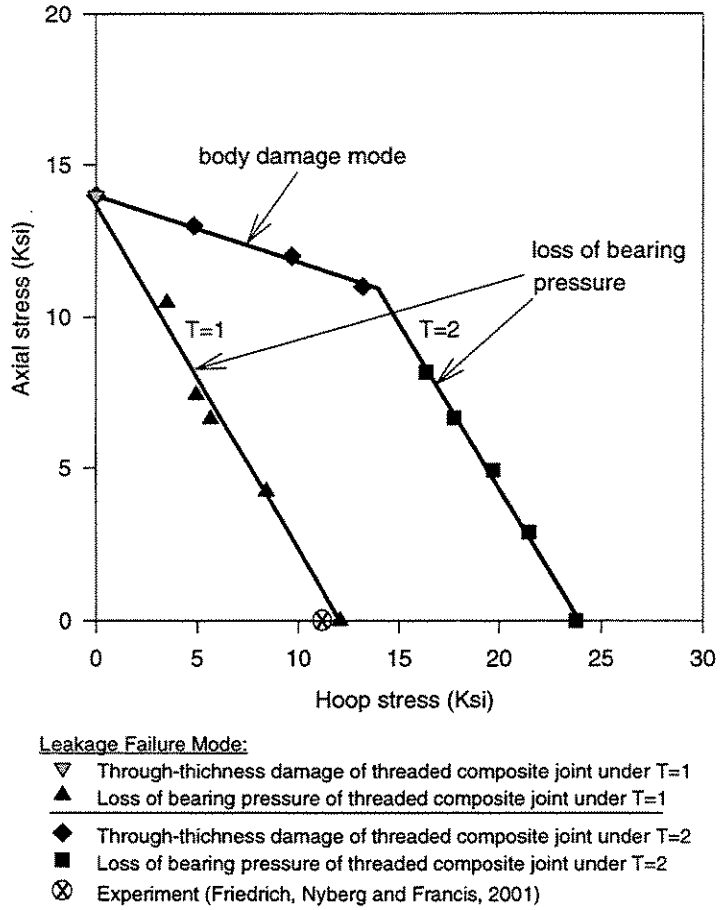

(a)

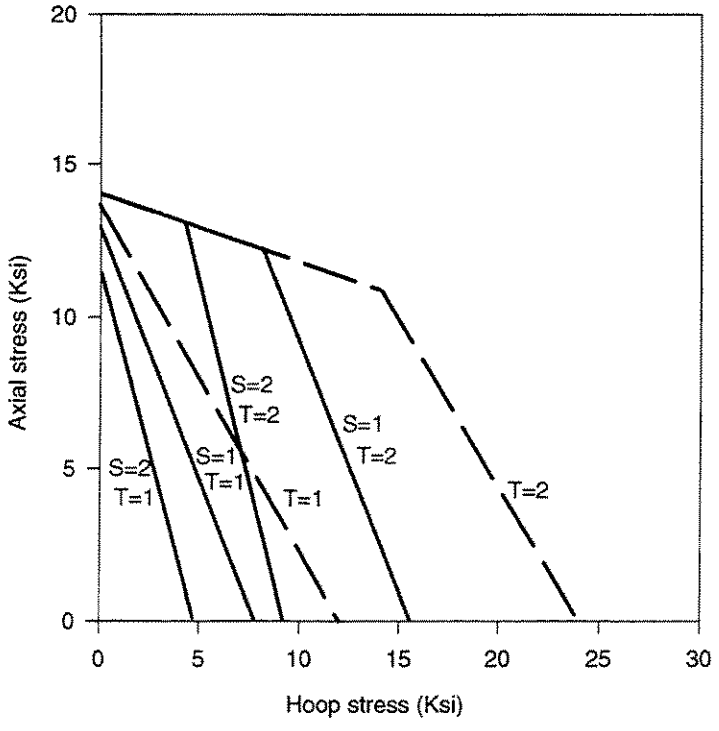

(b)

Fig. 7-29 (a) Failure and (b) Design Envelopes for Threaded Composite Joint under Makeup Loading: T=1 and T=2.

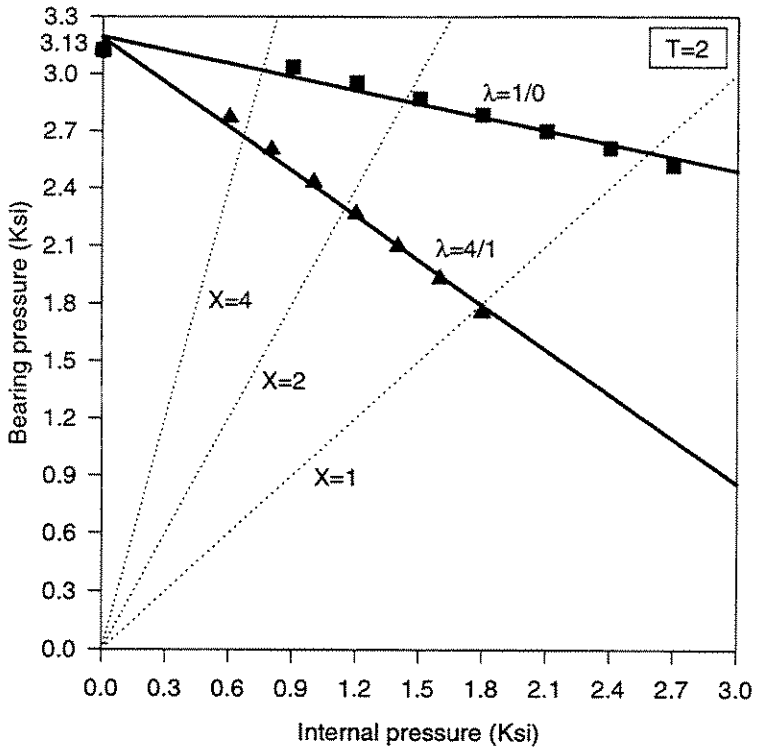

(a)

Fig. 7-30 (a) Bearing Pressure Versus Internal Pressure for Thicker-Box Joint (ξ=2) at T=2.

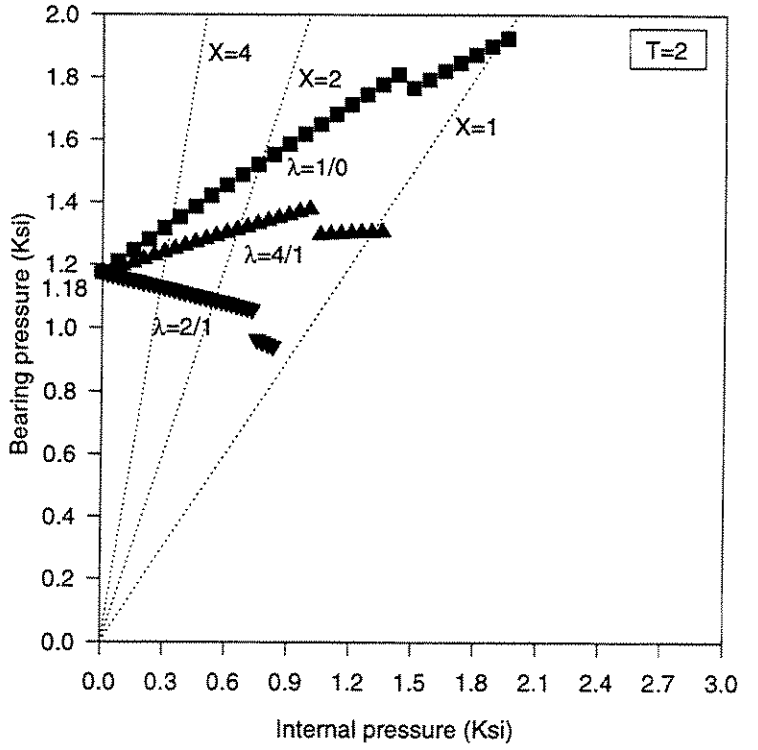

(b)

Fig. 7-30 (b) Bearing Pressure Versus Internal Pressure for Thinner-Pin Joint (ξ=1/2) at T=2.

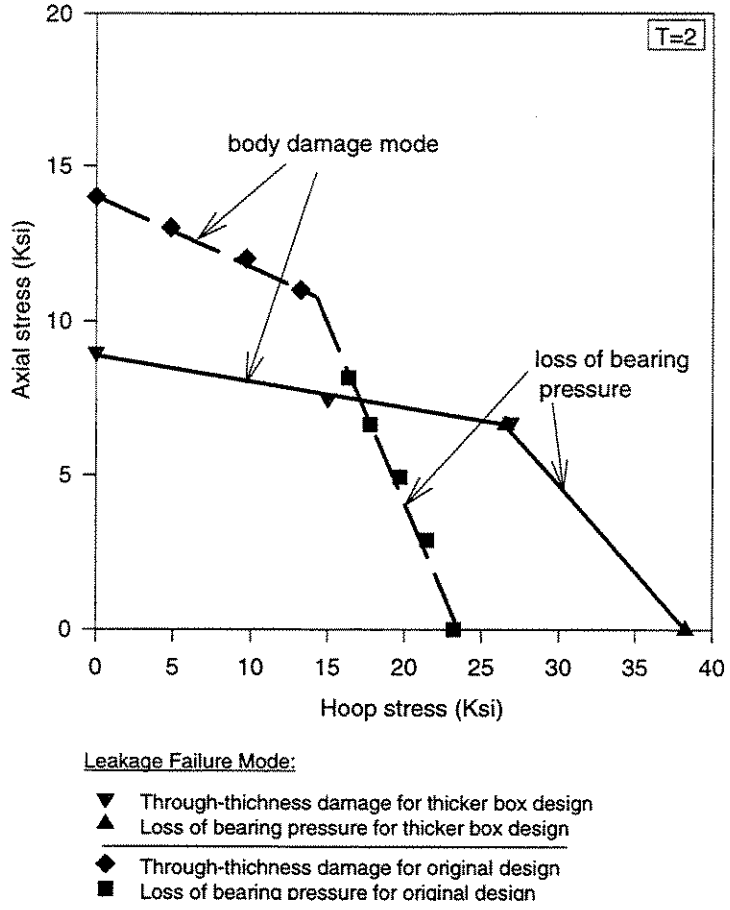

(a)

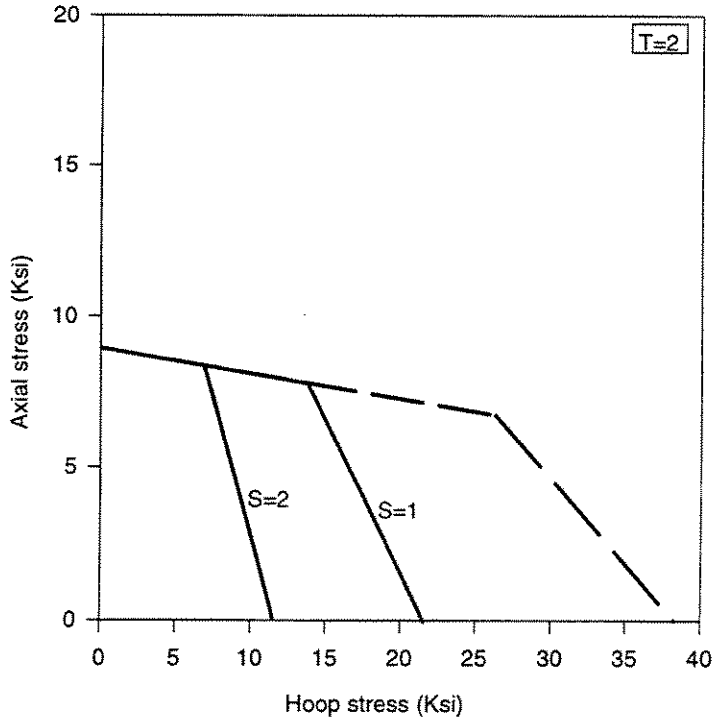

(b)

Fig. 7-31 (a) Failure and (b) Design Envelopes for Thicker-Box Joint under Makeup Loading, T=2.

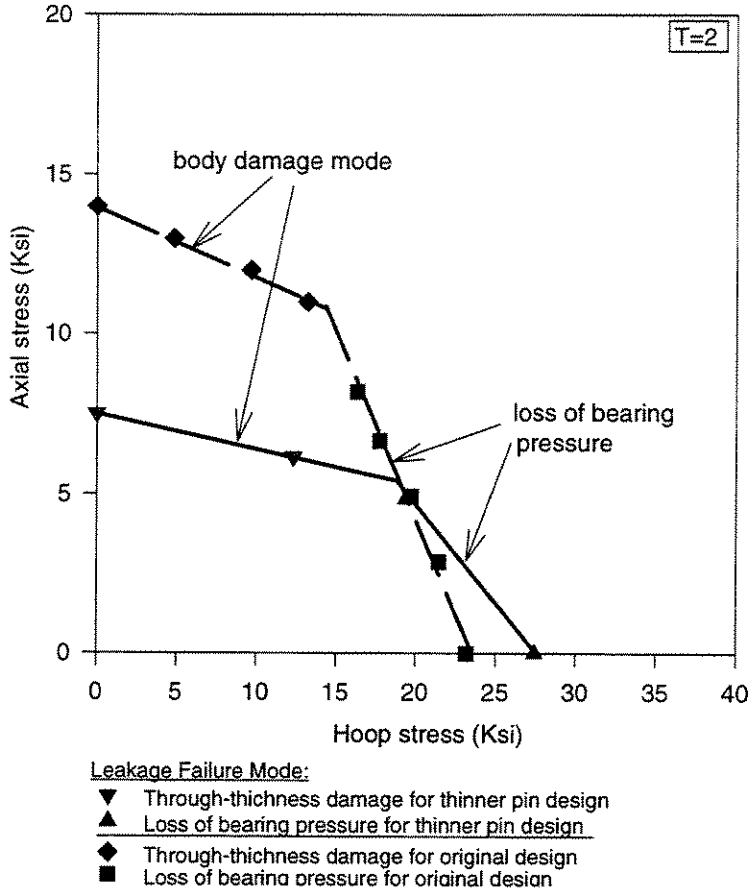

(a)

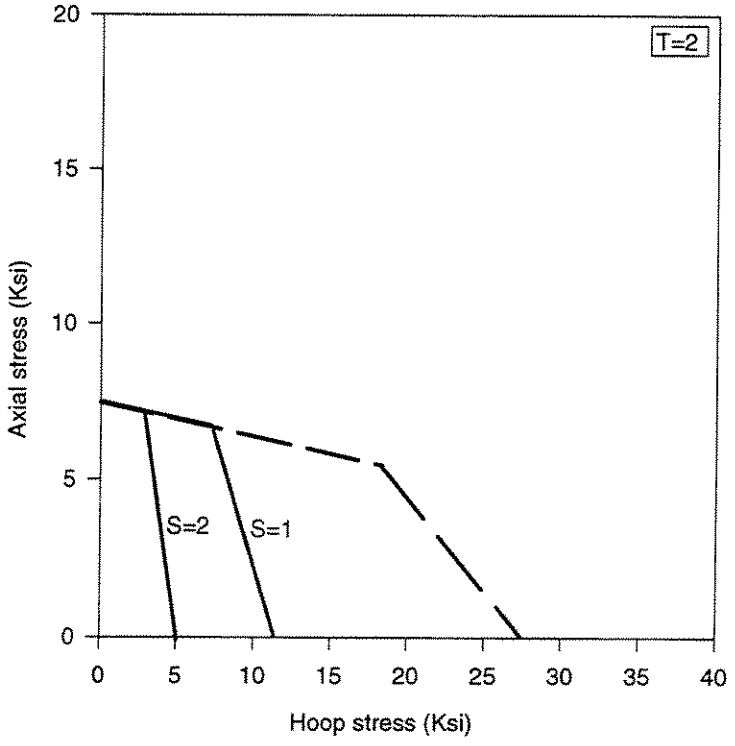

(b)

Fig. 7-32 (a) Failure and (b) Design Envelopes for Thinner-Pin Joint under Makeup Loading, T=2.

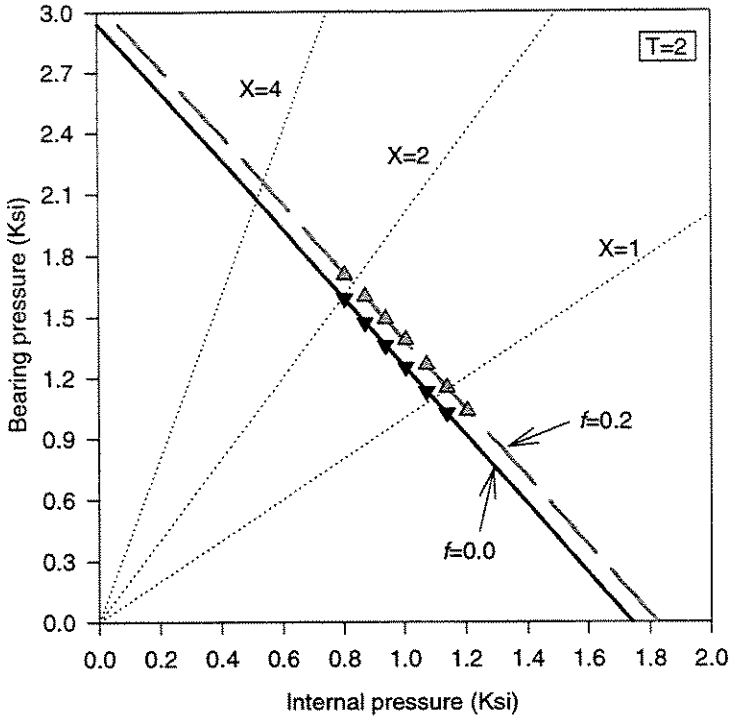

Fig. 7-33 Effect of Thread Surface Friction on Bearing Pressure Development in Threaded Composite Joint (Original Design; λ=2:1 and T=2).

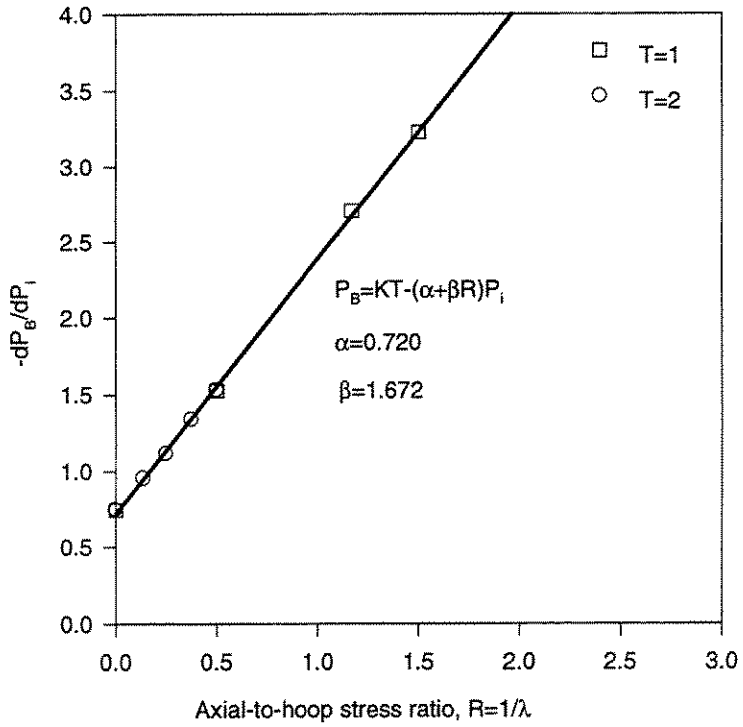

Fig. 7-34 Relationship among Thread Bearing Pressure, Internal Pressure and Stress Biaxiality Ratio for Leakage Failure of Threaded Composite Joint.

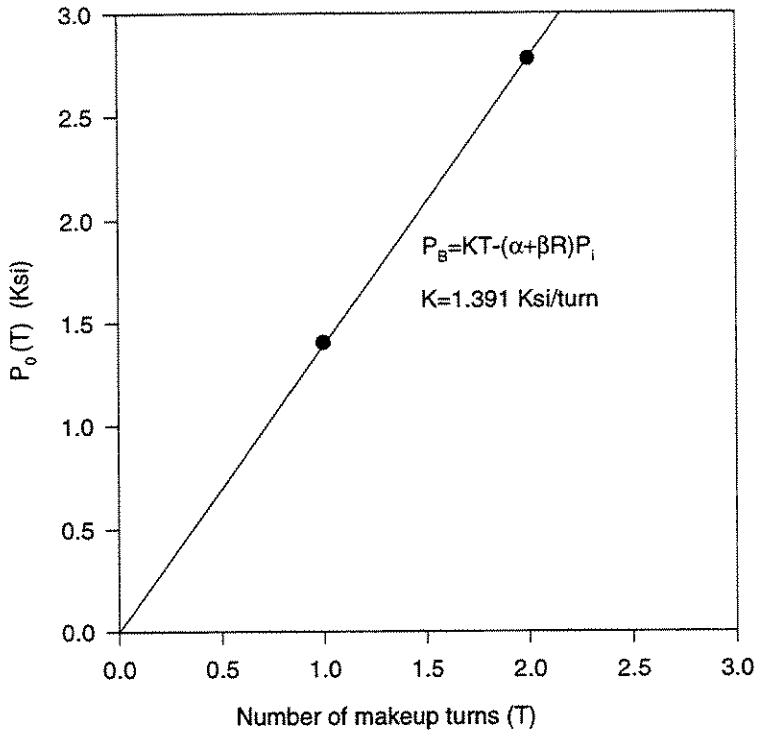

Fig. 7-35 Effect of Makeup Turns on Thread Bearing Pressure in Composite Joint without External Loading (Original Design).

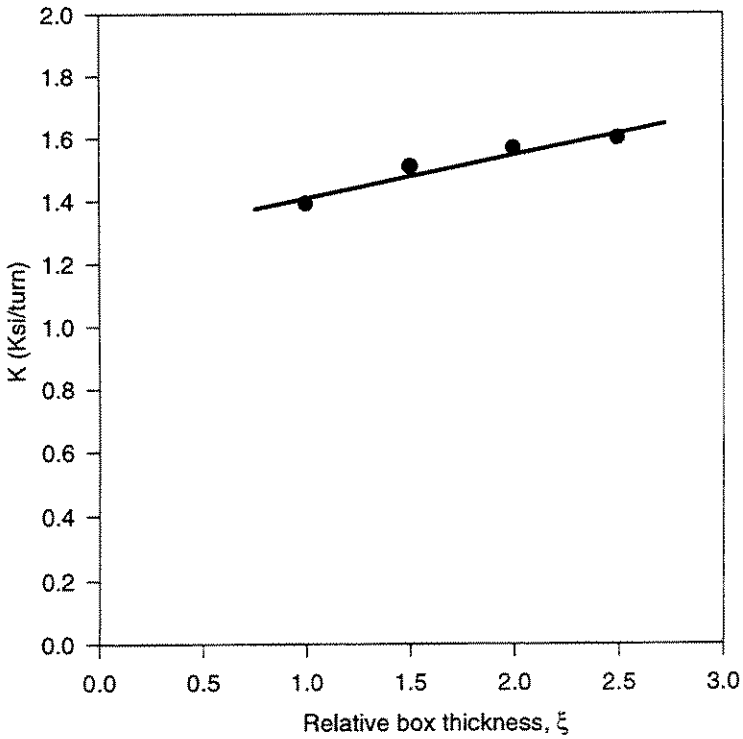

Fig. 7-36 Dependence of K on Relative Box Wall Thickness.

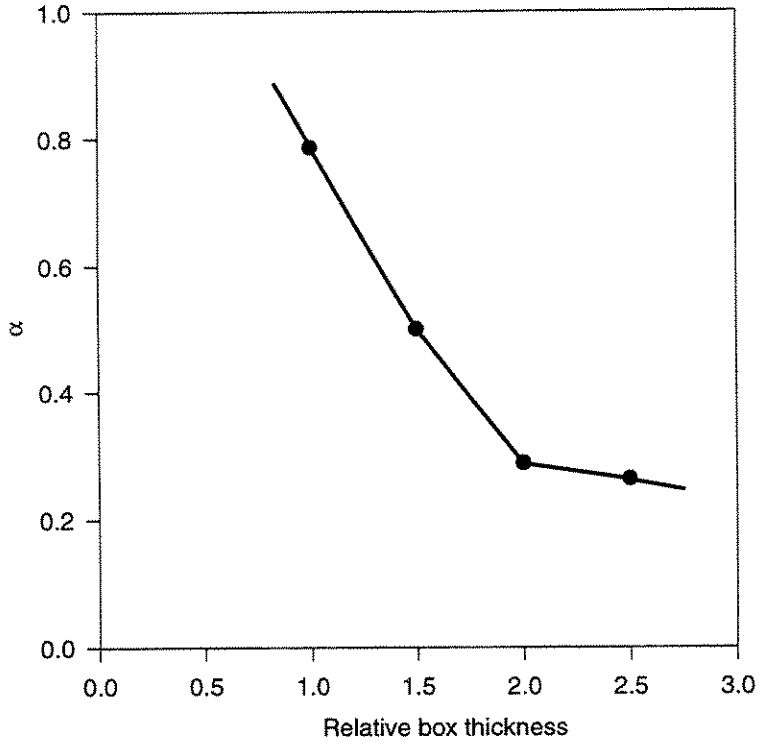

Fig. 7-37 Dependence of α on Relative Box Wall Thickness.

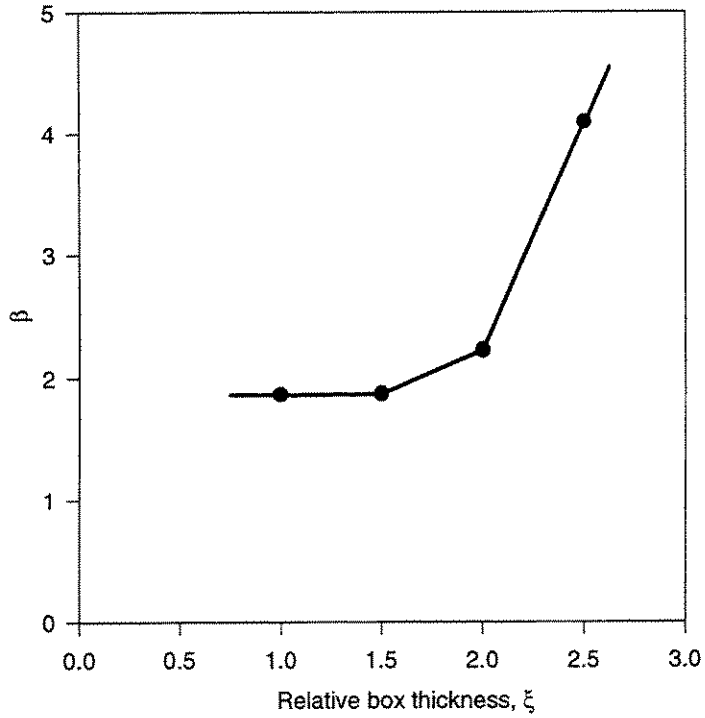

Fig. 7-38 Dependence of β on Relative Box Wall Thickness.

12. APPENDIX

I. DAMAGE EVOLUTION AND ASSOCIATED DEGRADATION IN COMPOSITE JOINT LEAKAGE

I.1 Damage Evolution at the Ply Level

It is recognized that fibers may be broken under tension or buckled under compression. The following expressions are used for evaluation of the complementary energy densities of fiber-dominated ply failure under tension and compression, respectively:

$$w_c^{(f)} = \frac{1}{2E_{11}(1-D_t^{(f)})}\sigma_{11}^2 + \frac{1}{2E_{22}}(\sigma_{22}^2+\sigma_{33}^2) - \frac{\nu_{12}}{E_{22}}(\sigma_{11}\sigma_{22}+\sigma_{11}\sigma_{33}) - \frac{\nu_{23}}{E_{22}}\sigma_{22}\sigma_{33} + \frac{1}{2G_{12}}(\tau_{12}^2+\tau_{13}^2) \tag{I-1a}$$

$$w_c^{(f)} = \frac{1}{2E_{11}(1-D_c^{(f)})}\sigma_{11}^2 + \frac{1}{2E_{22}}(\sigma_{22}^2+\sigma_{33}^2) - \frac{\nu_{12}}{E_{22}}(\sigma_{11}\sigma_{22}+\sigma_{11}\sigma_{33}) - \frac{\nu_{23}}{E_{22}}\sigma_{22}\sigma_{33} + \frac{1}{2G_{12}}(\tau_{12}^2+\tau_{13}^2) \tag{I-1b}$$

where subscripts 1, 2 ,3 represent directions along and transverse to the fiber direction; $D_t^{(f)}$ is a damage variable for fiber-dominated tensile failure mode, and $D_c^{(f)}$ is a damage variable for fiber-dominated compressive failure mode.

The well-known damage energy release rates $Y_t^{(f)}$ and $Y_c^{(f)}$ corresponding to $D_t^{(f)}$ and $D_c^{(f)}$ are obtained as

$$Y_t^{(f)} = \frac{\partial w_c^{(f)}}{\partial D_t^{(f)}} = \frac{\sigma_{11}^2}{2E_{11}(1-D_t^{(f)})^2} \tag{I-2a}$$

$$Y_c^{(f)} = \frac{\partial w_c^{(f)}}{\partial D_c^{(f)}} = \frac{\sigma_{11}^2}{2E_{11}(1-D_c^{(f)})^2} \tag{I-2b}$$

The ply composite fails in fiber-dominated tensile or compressive modes as the damage variables reach their critical values:

$$D_t^{(f)} = D_{tc}^{(f)} \quad \text{as } \sigma_{11}^{(f)} \geq 0 \tag{I-3a}$$

$$D_c^{(f)} = D_{cc}^{(f)} \quad \text{as } \sigma_{11}^{(f)} < 0 \tag{I-3b}$$

The polymer matrix composite may develop microcracking, or collapse in shear (Wang & Srinivasan, 1996) under mechanical loading. The damage variables corresponding to these damage mechanisms are introduced in the complementary energy function as

$$w_c^{(m)} = \frac{1}{2E_{11}}\sigma_{11}^2 + \frac{1}{2E_{22}(1-D_{22}^{(m)})}\sigma_{22}^2 + \frac{1}{2E_{22}(1-D_{33}^{(m)})}\sigma_{33}^2 - \frac{\nu_{23}}{E_{22}}\sigma_{22}\sigma_{33}$$
$$-\frac{\nu_{12}}{E_{22}}(\sigma_{11}\sigma_{22}+\sigma_{11}\sigma_{33}) + \frac{1}{2G_{12}(1-D_{12}^{(m)})}\tau_{12}^2 + \frac{1}{2G_{12}(1-D_{13}^{(m)})}\tau_{13}^2 \tag{I-4}$$

where $D_{22}^{(m)}$ and $D_{33}^{(m)}$ are damage variables for the matrix-dominated damage by transverse tensile stresses, and $D_{12}^{(m)}$ and $D_{13}^{(m)}$ are damage variables for the matrix-dominated damage by longitudinal shear stresses.

The damage energy release rates can be expressed in terms of these damage variables as

$$Y_{22}^{(m)} = \frac{\partial w_c^{(m)}}{\partial D_{22}^{(m)}} = \frac{\sigma_{22}^2}{2E_{22}(1-D_{22}^{(m)})^2} \tag{I-5a}$$

$$Y_{33}^{(m)} = \frac{\partial w_c^{(m)}}{\partial D_{33}^{(m)}} = \frac{\sigma_{33}^2}{2E_{22}(1-D_{33}^{(m)})^2} \tag{I-5b}$$

$$Y_{12}^{(m)} = \frac{\partial w_c^{(m)}}{\partial D_{12}^{(m)}} = \frac{\sigma_{12}^2}{2G_{12}(1-D_{12}^{(m)})^2} \tag{I-5c}$$

$$Y_{13}^{(m)} = \frac{\partial w_c^{(m)}}{\partial D_{13}^{(m)}} = \frac{\sigma_{13}^2}{2G_{12}(1-D_{13}^{(m)})^2} \tag{I-5d}$$

In Region I ($\sigma_{22} \geq 0$), where matrix-dominated damage occurs due to combined transverse tensile and longitudinal shear stresses, we have

$$Y_I^{(m)} = \frac{\partial w_c^{(m)}}{\partial D_I^{(m)}} = \frac{a^{(I)}\sigma_{22}^2}{2E_{22}(1-a^{(I)}D_I^{(m)})^2} + \frac{b^{(I)}\sigma_{12}^2}{2G_{12}(1-b^{(I)}D_I^{(m)})^2} \tag{I-6}$$

where the coupling between $D_{22}^{(m)}$ and $D_{12}^{(m)}$ are accounted for by $(D_{22}^{(m)}, D_{12}^{(m)}) = (a^{(I)}, b^{(I)})D_I^{(m)}$ in Region I.

Failure occurs as $D_I^{(m)}$ reaches a critical value, that is,

$$D_I^{(m)} = D_{Ic} \tag{I-7}$$

In Region II ($\sigma_2^* \leq \sigma_2 < 0$), where matrix-dominated damage occurs due to combined longitudinal shear and transverse compressive stresses, we have

$$Y_{II}^{(m)} = \frac{\partial w_c^{(m)}}{\partial D_{II}^{(m)}} = \frac{a^{(II)}\sigma_{22}^2}{2E_{22}(1-a^{(II)}D_{II}^{(m)})^2} + \frac{a^{(II)}\sigma_{12}^2}{2G_{12}(1-b^{(II)}D_{II}^{(m)})^2} \tag{I-8}$$

where the coupling between $D_{22}^{(m)}$ and $D_{12}^{(m)}$ are accounted for by $(D_{22}^{(m)}, D_{12}^{(m)}) = (a^{(II)}, b^{(II)})D_{II}^{(m)}$ in Region II.

Failure occurs as $D_{II}^{(m)}$ reaches a critical value, that is,

$$D_{II}^{(m)} = D_{IIc} \tag{I-9}$$

In Region III ($\sigma_2 < \sigma_2^* < 0$), where matrix-dominated damage occurs due to combined transverse compressive and longitudinal shear stresses, we have

$$Y_{III}^{(m)} = \frac{\partial w_c^{(m)}}{\partial D_{III}^{(m)}} = \frac{a^{(III)}\sigma_{22}^2}{2E_{22}(1-a^{(III)}D_{III}^{(m)})^2} + \frac{b^{(III)}\sigma_{12}^2}{2G_{12}(1-b^{(III)}D_{III}^{(m)})^2} \tag{I-10}$$

where the coupling between $D_{23}^{(m)}$ and $D_{12}^{(m)}$ are accounted for by $(D_{22}^{(m)}, D_{12}^{(m)}) = (a^{(III)}, b^{(III)})D_{III}^{(m)}$ in Region III.

Failure occurs as $D_{III}^{(m)}$ reaches a critical value, that is,

$$D_{III}^{(m)} = D_{IIIc} \tag{I-11}$$

Since no experimental characterization is currently available for multiaxial damage evolution in fiber composites, we may use the following damage potential from a related study (Lemaitre, 1996)

$$\Phi(Y^{(m)}) = Y^{(m)\eta^{(m)}/2} = \alpha^{(m)}D^{(m)} + \beta^{(m)}p + const \tag{I-12}$$

where p is the hydrostatic pressure in the transverse direction, and $\alpha^{(m)}$, $\beta^{(m)}$ and $\eta^{(m)}$ are material parameters.

I.2 Composite Tube Body and Thread Interface Damage

Since the composite tube body and thread interface may undergo debonding due to interfacial tension and shear, we introduce a damage variable of interface. The complementary energy density of the interface in the local interfacial coordinates can be expressed as

$$w_c^{(i)} = \frac{\tilde{S}_{11}\tilde{\sigma}_{11}^{(i)2}}{2(1-D_n^{(i)})} + \frac{\tilde{S}_{66}\tilde{\tau}_{12}^{(i)2}}{2(1-D_t^{(i)})} + \frac{\tilde{S}_{55}\tilde{\tau}_{13}^{(i)2}}{2(1-D_t^{(i)})} \tag{I-13}$$

The damage energy release rates in terms of $D_n^{(i)}$ and $D_t^{(i)}$ are

$$Y_n^{(i)} = \frac{\partial w_c^{(i)}}{\partial D_n^{(i)}} = \frac{\tilde{S}_{11}\tilde{\sigma}_{11}^{(i)2}}{2(1-D_n^{(i)})^2} \tag{I-14}$$

$$Y_t^{(i)} = \frac{\partial w_c^{(i)}}{\partial D_t^{(i)}} = \frac{\tilde{S}_{66}\tilde{\tau}_{12}^{(i)2} + \tilde{S}_{55}\tilde{\tau}_{13}^{(i)2}}{2(1-D_t^{(i)})^2} \tag{I-15}$$

When an interfacial damage occurs due to combined tensile and shear stresses, we have

$$Y^{(i)} = \frac{\partial w_c^{(i)}}{\partial D^{(i)}} = \tilde{a}\frac{\tilde{S}_{11}\tilde{\sigma}_{11}^{(i)2}}{2(1-D^{(i)})^2} + \tilde{b}\frac{\tilde{S}_{66}\tilde{\tau}_{12}^{(i)2} + \tilde{S}_{55}\tilde{\tau}_{13}^{(i)2}}{2(1-\tilde{a}D^{(i)})^2} \tag{I-16}$$

where the coupling between $D_n^{(i)}$ and $D_t^{(i)}$ are accounted for by $(D_n^{(i)}, D_t^{(i)}) = (\tilde{a}, \tilde{b})D^{(i)}$.

Failure occurs as $D^{(i)}$ reaches a critical value, that is,

$$D^{(i)} = D_c^{(i)} \tag{I-17}$$

Using of a similar form of dissipation potential as Eq. (I-12), we have

$$\Phi(Y^{(i)}) = Y^{(i)^{\eta^{(i)}}} = \alpha^{(i)} D^{(i)} + \beta^{(i)} p_n + const \tag{I-18}$$

where p_n is the normal pressure acting on the interface.

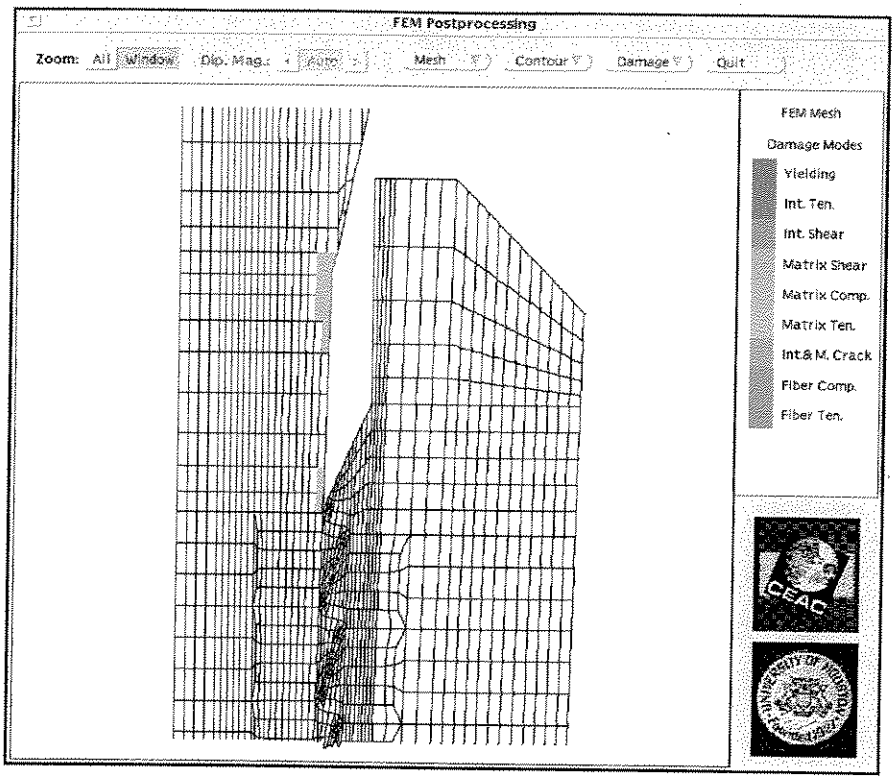
FEM Postprocessing
Zoom: All Window Dip. Mag.: 1 Zoom 2
Mesh
Contour
Damage
Quit
FEM Mesh
Damage Modes
Yielding
Int. Ten.
Int. Shear
Matrix Shear
Matrix Comp.
Matrix Ten.
Int.& M. Crack
Fiber Comp.
Fiber Ten.
CEAC

(a)

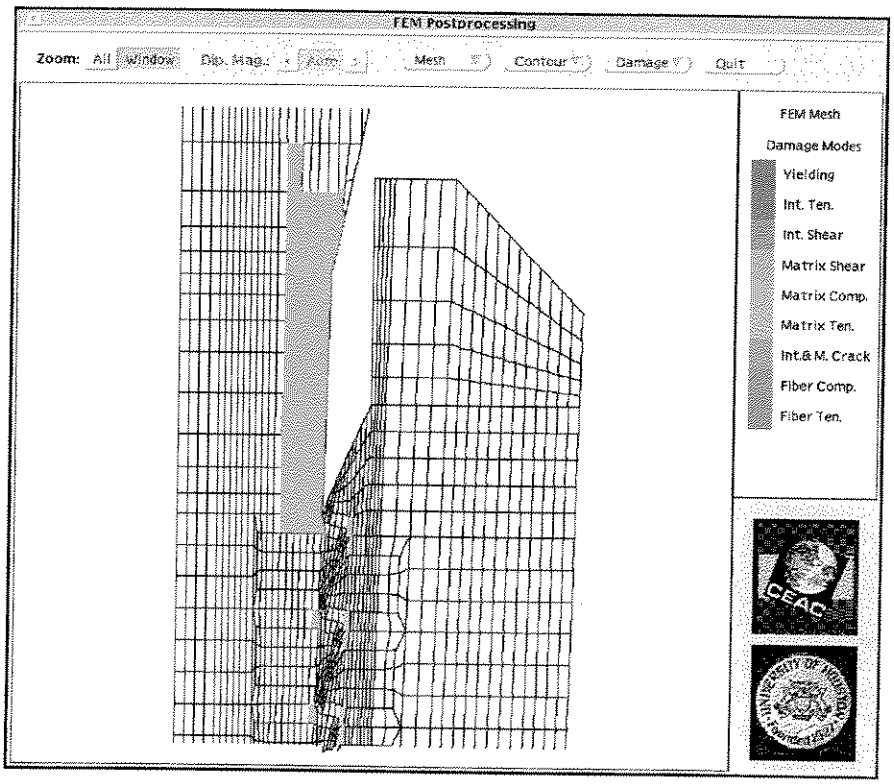
FEM Postprocessing
Zoom: All Window Dip. Mag.: 1 Zoom 2
Mesh
Contour
Damage
Quit
FEM Mesh
Damage Modes
Yielding
Int. Ten.
Int. Shear
Matrix Shear
Matrix Comp.
Matrix Ten.
Int.& M. Crack
Fiber Comp.
Fiber Ten.
CEAC

(b)

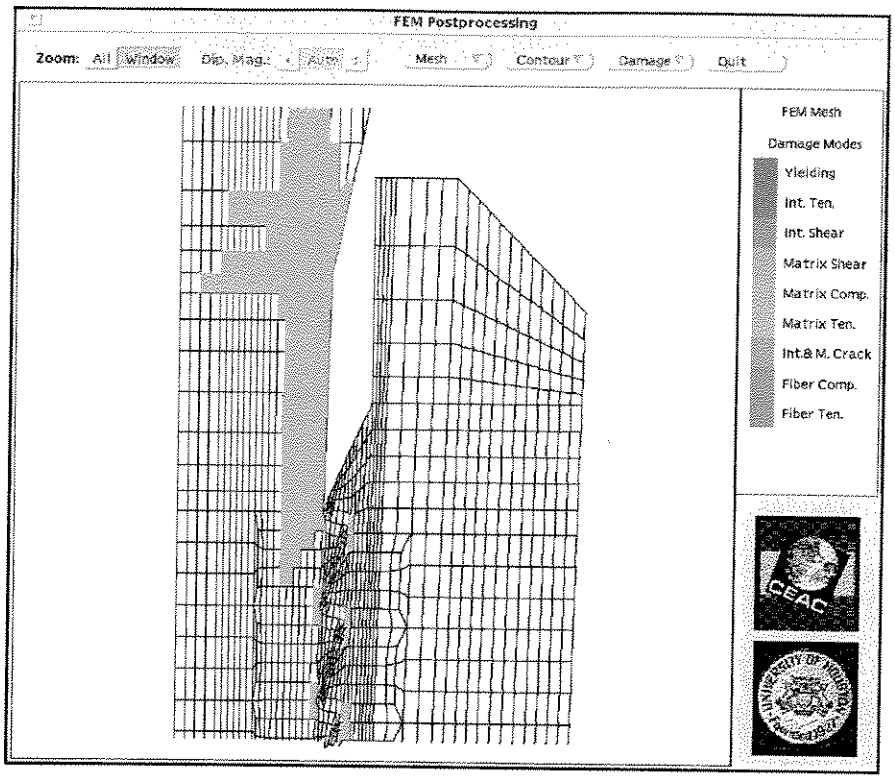

(c)

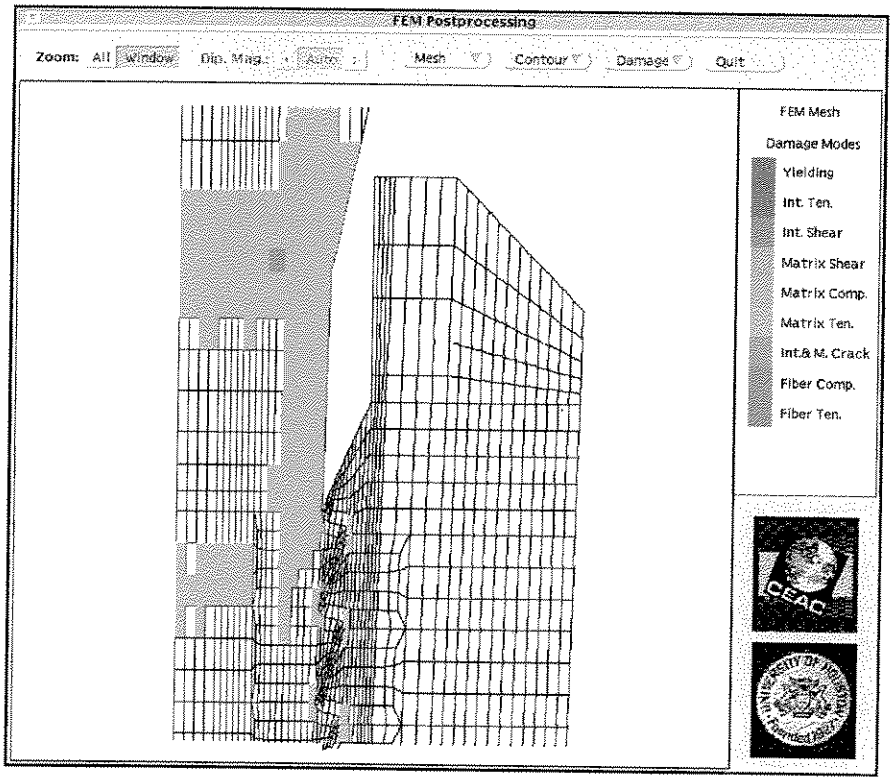

(d)

Fig.A-1 Damage Modes and Growth Near the End of Box Section Using Damage Mechanics Formulation under Axial Tension (T=2).
(a) σ_a=7 Ksi; (b) σ_a=11 Ksi; (c) σ_a=13.5 Ksi; (d) σ_a=14 Ksi

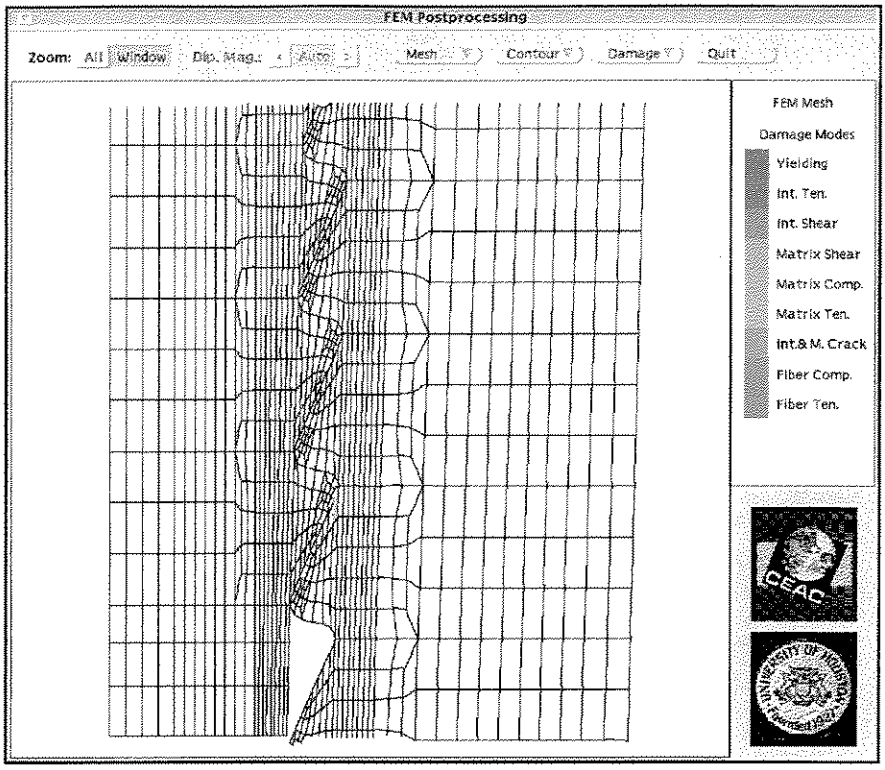
FEM Postprocessing
Zoom: All Window
Dip. Mag.:
Mesh
Contour
Damage
Quit
FEM Mesh
Damage Modes
Yielding
Int. Ten.
Int. Shear
Matrix Shear
Matrix Comp.
Matrix Ten.
Int.& M. Crack
Fiber Comp.
Fiber Ten.
CEAC

(a)

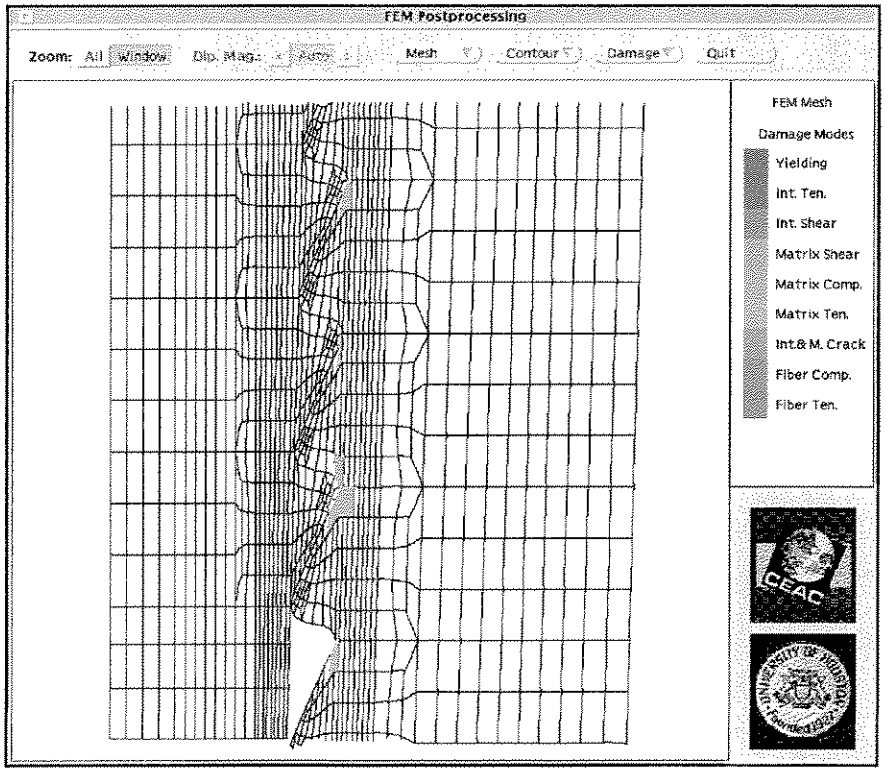
FEM Postprocessing
Zoom: All Window
Dip. Mag.:
Mesh
Contour
Damage
Quit
FEM Mesh
Damage Modes
Yielding
Int. Ten.
Int. Shear
Matrix Shear
Matrix Comp.
Matrix Ten.
Int.& M. Crack
Fiber Comp.
Fiber Ten.
CEAC

(b)

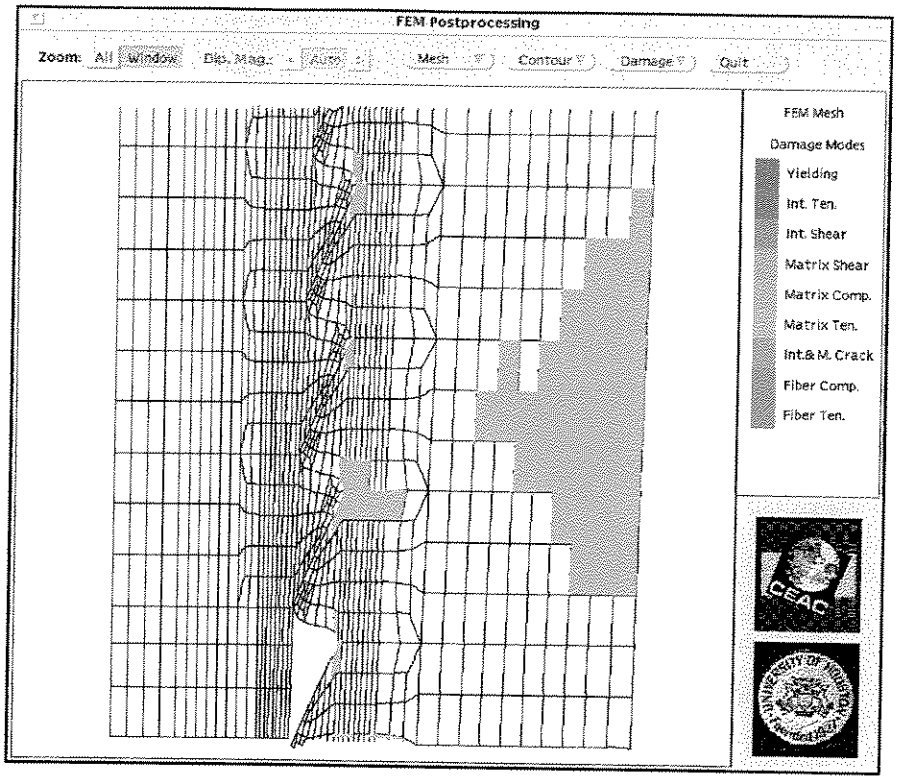

(c)

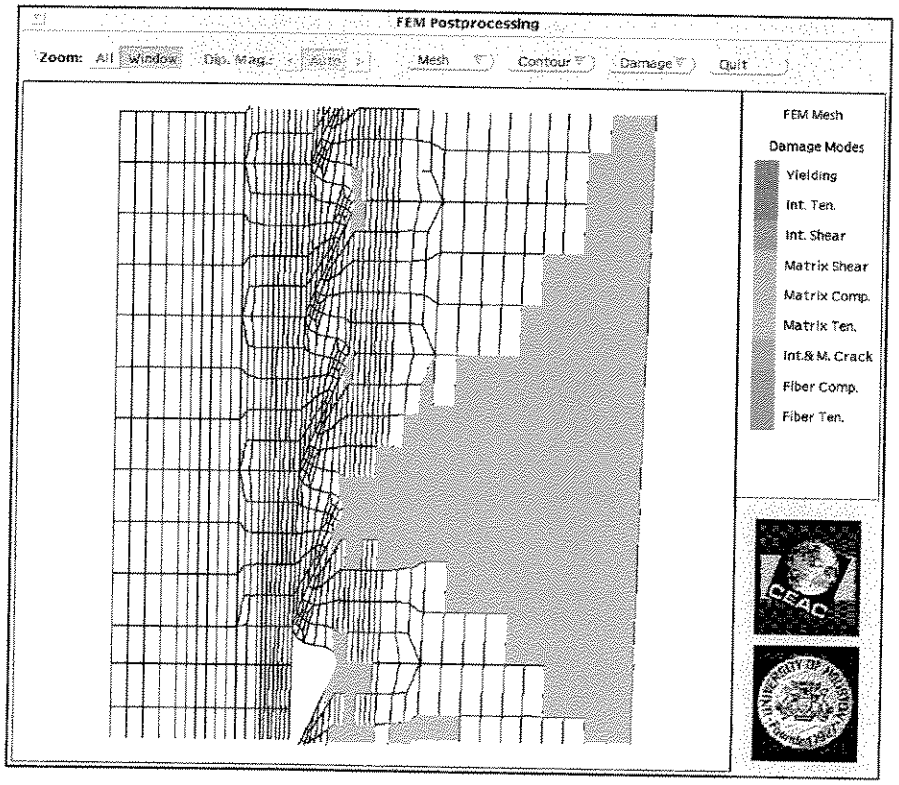

(d)

Fig.A-2 Damage Modes and Growth Near the End of Pin Section Using Damage Mechanics Formulation under Axial Tension (T=2).
(a) σ_a=7 Ksi; (b) σ_a=11 Ksi; (c) σ_a=13.5 Ksi; (d) σ_a=14 Ksi